Quaternary glucocorticoid receptor structure highlights allosteric interdomain communication

Sandra Postel, Lisa Wissler, Carina Johansson, Anders Gunnarsson, Euan Gordon, Barry Collins, Marie Castaldo, Christian Köhler, David Öling, Patrik Johansson, et al.

Quaternary GR structure highlights allosteric interdomain communication

Sandra Postel[1], Lisa Wissler[1], Carina A. Johansson[1], Anders Gunnarsson[1], Euan Gordon[2], Barry Collins[3], Marie Castaldo[2], Christian Köhler[3], David Öling[2], Patrik Johansson[1], Linda Fröderberg Roth[2], Brice Beinsteiner[4,5,6,7], Ian Dainty[3], Stephen Delaney[3], Bruno P. Klaholz[4,5,6,7], Isabelle M.L. Billas[4,5,6,7], Karl Edman[1]

[1]Mechanistic and Structural Biology, Discovery Sciences, R&D, AstraZeneca, Gothenburg, Sweden

[2]Discovery Biology, Discovery Sciences, R&D, AstraZeneca, Gothenburg, Sweden

[3]Research and Early Development, Respiratory and Immunology, BioPharmaceuticals R&D, AstraZeneca, Gothenburg, Sweden

[4] IGBMC (Institute of Genetics and of Molecular and Cellular Biology), Illkirch, France

[5] Université de Strasbourg, Illkirch, France

[6] Institut National de la Santé et de la Recherche Médicale (INSERM) U1258, Illkirch, France

[7] Centre National de la Recherche Scientifique (CNRS) UMR 7104, Illkirch, France

Abstract

The glucocorticoid receptor (GR) is a ligand activated transcription factor that binds DNA and assembles context dependent coregulator complexes to regulate gene transcription. GR agonists are widely prescribed to patients with inflammatory and autoimmune diseases. Here, we determine the first high resolution, multi-domain structures of GR in complex with ligand, DNA and a coregulator peptide. The structures reveal how the receptor forms an asymmetric dimer on the DNA and provide a detailed view of the domain interactions within and across the two monomers. Hydrogen deuterium exchange and DNA binding experiments

demonstrate that ligand dependent structural changes are communicated across the different domains in the full-length receptor. Based on the structural analysis, we design mutant receptor constructs and functional assays to validate the signaling pathways identified in the structures. This study demonstrates how GR forms a distinct architecture on DNA and how signal transmission can be modulated by the ligand pharmacophore. The results provide a platform where we can build a new level of understanding for how receptor modifications can drive disease progression and offer key insight for future drug design.

Introduction

The glucocorticoid receptor (GR) is a ubiquitously expressed nuclear hormone receptor. Together with the androgen, progesterone and mineralocorticoid receptors, GR forms the keto-steroid receptor subfamily which evolved from an estrogen receptor (ER) like ancestor in vertebrates[1]. GR is activated through endocrine signaling by the glucocorticoid hormone cortisol, and is of fundamental importance for development, skeletal growth, behavior, glucose homeostasis and inflammation.

GR comprises a large, disordered N-terminal domain, a DNA-binding domain (DBD) and a ligand-binding domain (LBD). In the apo state, GR primarily resides in a chaperone complex in the cytoplasm. Ligand activation triggers nuclear translocation and receptor binding to specific DNA sequences. On the DNA, GR recruits co-regulators and other transcription factors in a context dependent manner to ultimately repress or activate transcription of a large set of target genes[2]. As such, GR provides a plastic scaffold which integrates signaling input from the ligand pharmacophore, the sequence of the DNA and post-translational

modifications and the outcome of the signaling event is governed by the identity of the assembled co-regulators.

Signaling efficiency is dependent on comprehensive allosteric networks that enable communication in between distinct functional sites across the receptor domains. GR typically binds as a dimer to the canonical GR binding sequence (GBS), which is an imperfect palindromic hexameric DNA sequence repeat, separated by a 3-nucleotide spacer[3]. However, GR can also bind as a monomer to a canonical half-site[4] or as discrete monomers on opposite sides of the DNA to an inverted repeat sequence[5]. This adds a layer of combinatorial flexibility and contributes to signaling diversity, but also suggests that the protein interfaces must be able to adapt to different boundary conditions.

To date, structural studies have focused on the individual domains within the receptor. Studies of the DBD in complex with DNA have demonstrated how the nucleotide sequence drives structural rearrangement within the DBD dimer[6]. The structures of the LBD in complex with a wide array of ligands have highlighted the plasticity of the ligand binding pocket[7]. However, a full understanding of the allosteric transmission in between the ligand and DNA binding events and effects on co-regulator recruitment requires structural information from a multi-domain construct.

Here we present the crystal structures of a GR construct (residues 385-777, encompassing the DBD and LDB) in complex with the agonists velsecorat[8] and fluticasone furoate[9], a natural GBS and a co-regulator peptide. These are the first high-resolution multidomain structures of a steroid receptor and reveal how the receptor forms a unique architecture on the DNA.

Results

To determine the multidomain structure of GR, we expressed and purified several GR constructs (Fig. 1a) in the presence of the strong agonists velsecorat (Vel), fluticasone furoate (FF), or dexamethasone (Dex) (Fig. 1b). All three ligands exhibit strong anti-inflammatory responses, inhibiting lipopolysaccharide (LPS) induced tumor necrosis factor α (TNFα) secretion in human whole blood with an IC_{50} of 10.74 nM, 3.63 nM and 34.70 nM, respectively (Fig. 1c), and have demonstrated clinical efficacy in a range of disease indications[10-12].

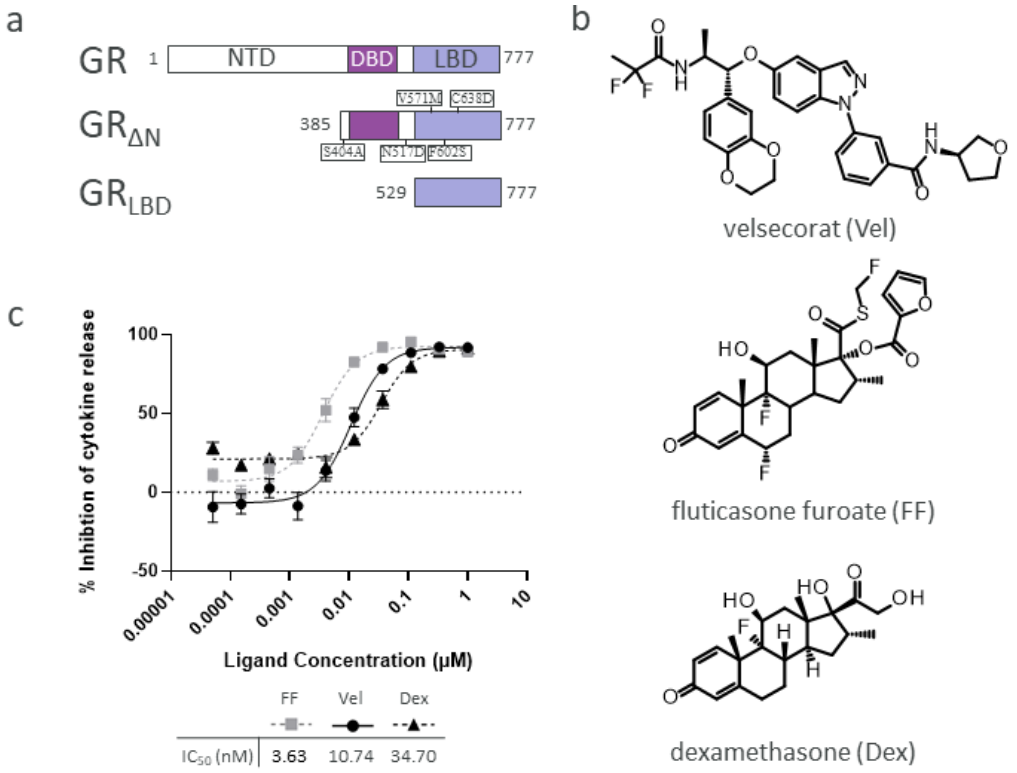

Figure 1 | GR protein constructs and agonists used in this study. a, GR protein constructs used in this study. The $GR_{\Delta N}$ construct includes five stabilizing mutants highlighted in the schematic. **b,** The chemical structure of the GR agonists velsecorat, fluticasone furoate and dexamethasone. **c,** Velsecorat, fluticasone furoate and dexamethasone inhibit LPS induced

TNFα production in human whole blood. Data points are mean ± s.e.m. of six replicates from three donors.

The purified receptors were then mixed with dsDNA and coregulator peptide to obtain quaternary complexes (Extended Data Fig. 1). The $GR_{\Delta N}$ contains 5 stabilizing mutants (Fig. 1a) and yielded diffracting crystals with both velsecorat and fluticasone furoate. The highest resolution structure (2.5 Å, Extended Data Table 1) was obtained from the $GR_{\Delta N}$ construct in complex with velsecorat [$GR_{\Delta N}$(Vel)], a GBS from the serum and glucocorticoid-regulated kinase-1 (*SGK-1*) promoter, and a peptide (residues 134-154) derived from the co-regulator peroxisome proliferator-activated receptor ɣ coactivator 1-α (PGC1α).

The structure reveals that the LBD dimer is asymmetrically placed on top of the center of the DBD dimer resulting in a shifted tetrahedral architecture on the DNA (Fig. 2). In the crystal lattice, there are two alternative LBD dimer interfaces; one consisting of two separate regions spanning the N-terminal end of H10/11 and H6-H7 (Fig. 2a, b, d), and one primarily mediated by H1 (Fig. 2c). We could not detect any electron density for the linker residues (residues 489-525) in between the LBD and DBD in any of our structures, which is likely due to the flexible nature of this region[13]. However, the H10/11 interface partially overlaps with the canonical ER dimer interface[14] and exhibits a larger total buried surface area of 904.4 $Å^2$ (compared to 710.2 for the H1 dimer interface). We propose that this is the primary LBD dimer for GR activation on the SGK-1 GBS. The LBD dimer is tilted relative to the DBD dimer (Fig. 2a, b), which positions the LBD N-termini in proximity of the DBD C-termini. Based on distances, number of missing residues and space constraints between the C-terminus of the DBD domains and the N-terminus of LBD domains, we suggest that DBD1 is

connected to LBD1 and DBD2 to LBD2, but the alternative connectivity cannot be fully excluded.

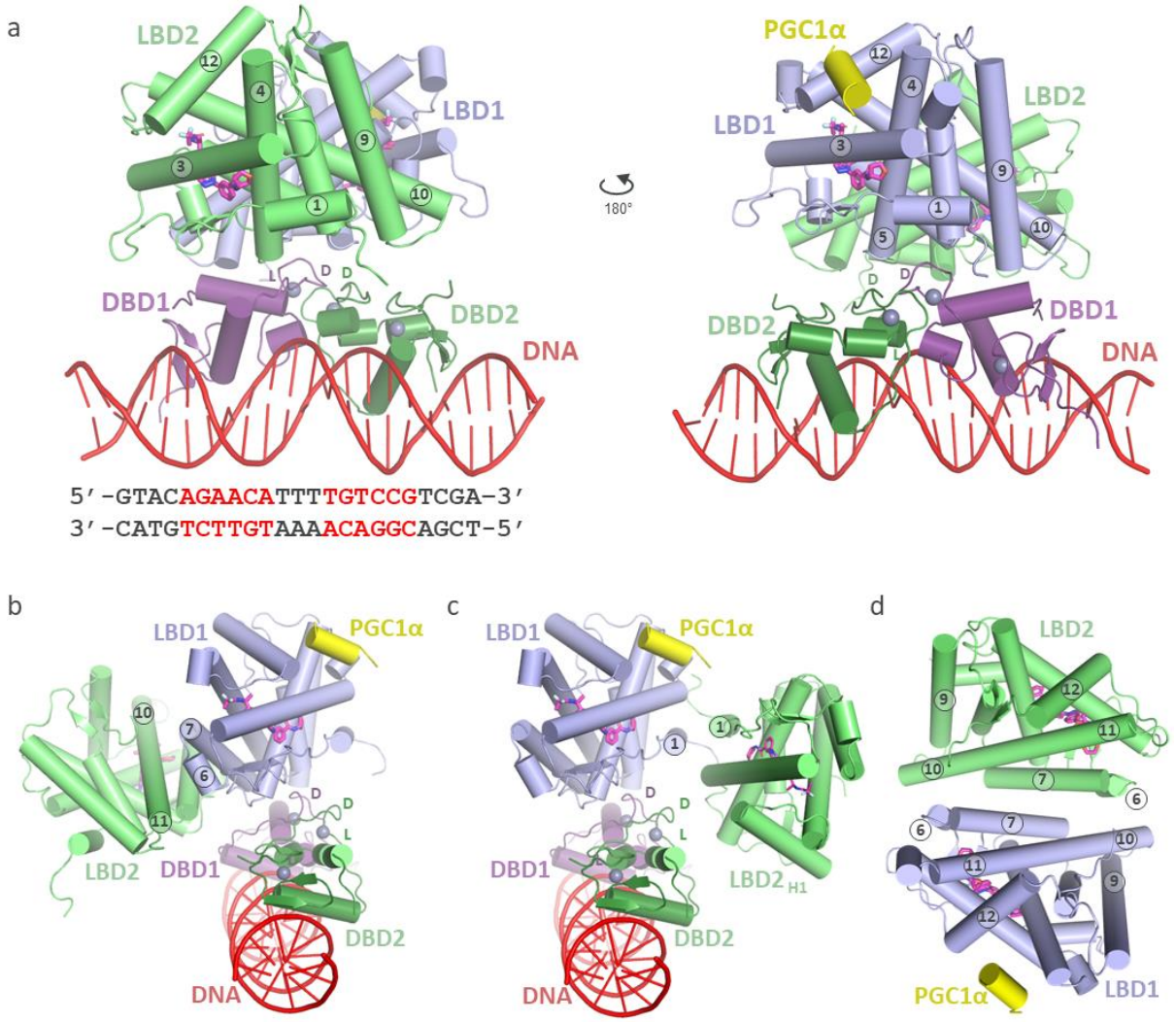

Figure 2 | Structure of $GR_{\Delta N}$(Vel) in complex with *SGK* and PGC1α$_{134\text{-}154}$.

a, b, High resolution crystal structure of $GR_{\Delta N}$(Vel) in complex with dsDNA *SGK* (red) and the coactivator peptide PGC1α$_{134\text{-}154}$ (yellow). Velsecorat is shown as a stick model (magenta) and Zn atoms as spheres (gray). GR LBD helix numbering is annotated within the circles. The DBD dimerization loops and lever arms are marked D and L, respectively. The nucleotide sequence of the SGK GBS is highlighted with the two half-sites in red. **c**, The alternative LBD dimer (LBD1: LBD2$_{H1}$) in the crystallographic lattice in which the LBD-LBD interface is mediated by H1 interactions. **d**, Top view of the head-to-tail LBD dimer interface as shown in **a** and **b**.

The asymmetric placement of the LBD dimer on the DBD dimerization loops (D-loops) results in LBD1 interacting with the D-loops of both DBD1 and DBD2 with a combined buried surface area of 731 Å^2, while LBD2 only contacts the lever arm of DBD1 with a buried surface area of 145.2 Å^2 (Fig. 2a, b). This arrangement of the LBD dimer on the DBD dimer agrees with NMR studies of DBD complexes with multiple GBSs which, combined with functional cell assay data, suggested that both the D-loop and the lever arm could be involved in inter-domain communication[3,6]. In addition, NMR studies of WT GR LBD revealed an allosteric pathway from the ligand binding pocket to the N-terminal end of helix 1[15]. In our structure the LBD1 H1 is in direct contact with the DBD D-loops, and likely forms a communication network that links the DNA sequence to the ligand pharmacophore.

In the keto-steroid receptors, a conserved C-terminal extension (residues 767-777) prevents formation of the stable head-to-head LBD dimer observed for ER[16]. In contrast, the $GR_{\Delta N}$(Vel) LBDs form a unique head-to-tail dimer (Fig. 2c), which has not been observed in any GR LBD structure to date[17]. The LBD construct alone remains predominantly monomeric in solution[18] and formation of a relevant LBD dimer likely requires DNA binding (Extended Data Fig. 1).

To study the degree of sequence conservation of the LBD interface residues, we collected 34 GR and 34 reference ER sequences from vertebrates with a similar degree of sequence diversity (see Materials and Methods and Extended Data Fig. 3 and 4). We then mapped the mean pairwise column identity of each residue onto the corresponding LBD structure surface (ER PDB: 3ERD) with the dimerization interface outlined in red (Fig. 3a, b). The ER LBD forms a stable dimer in solution with a total buried surface area of 1581.5 Å^2. The ER dimer

interface and the conservation pattern are strikingly different from the ones observed in GR. However, when superimposing the ER LBD dimer onto the GR LBD dimer (Fig. 3c), the GR dimer interface has merely shifted to an overlapping position due to the GR LBD1 C-terminus shielding the original ER interface. In addition, both interfaces exhibit a similar degree of total conservation, with an average mean pairwise column identity of 0.70 and 0.72 for GR and ER, respectively. A detailed investigation of the GR LBD dimerization interface reveals a cluster of conserved polar resides forming a network of interactions across the two domains (Fig. 3d). Analysis of other key interfaces suggests that the LBD regions facing the DBD dimer (Extended Data Fig. 5a) and the coregulator binding site (AF-2, Extended Data Fig. 5b) are highly conserved.

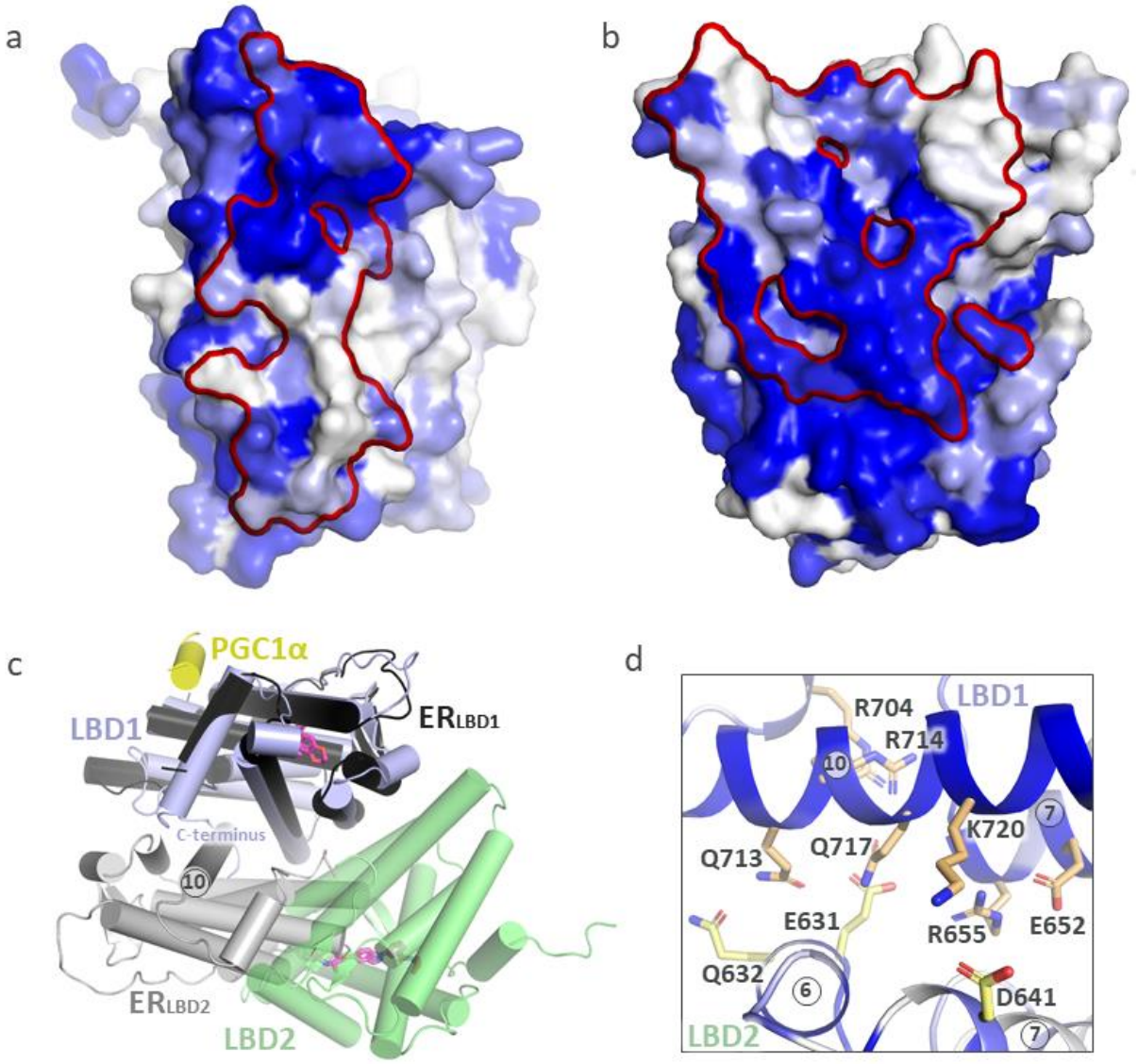

Figure 3 a, Degree of conservation of GR and **b,** ER. LBD residues colored according to column identity between 0.4 (white) and 1.0 (blue) with LBD dimerization interfaces outlined in red (using a 5Å distance cutoff). **c,** The ER LBD dimer (in black and gray) superposed on the GR LBD dimer presented in this study (in blue and green). The structures have been overlaid using GR LBD1 as reference. **d,** Highly conserved polar residues in the GR LBD dimer interface.

The dimer we observe is distinct from the ones reported in published structures of the GR LBD alone. The dimer interface proposed in the first GR LBD publication includes the loop

in between H1 and H3, the antiparallel β-sheet region and the C-terminal end of H5[19]. In our structure, this area is directed towards the DBD-DNA for both LBD1 and LBD2, preventing formation of this interface in the crystal lattice. A recent evaluation of all GR LBD structures to date[17] highlighted that H9 forms significant crystal contacts either in a parallel or anti-parallel fashion in many of the LBD structures. In the quaternary structure we present here, this interaction is obstructed by dsDNA from crystallographic neighbors in the lattice. The most prevalent potential dimer interaction in the GR LBD structures, however, is the option mediated by H1[17]. This interface is also present in our lattice (Fig. 2c). It has been proposed that GR may form transient higher-order oligomeric states[20,21]. It is plausible that the H1 interaction (or even H9 interactions) may mediate formation of tetramers or even higher-order states (Extended Data Fig. 6), bringing distal GBS together in a folded assembly.

The best characterized co-regulator interaction surface is the activation function 2 (AF-2), at the intersect of LBD helices 3, 4 and 12 (H3, H4 and H12), where the canonical co-activator LxxLL peptide sequence motif binds upon agonist activation. The LBD arrangement presented here, aligns both AF-2 surfaces on the outside of the tetrahedron, accessible for co-regulator binding. However, while both LBDs have H12 arranged in an active position, only the LBD1 AF-2 site is occupied by the PGC1α peptide (Fig. 2a, b). Crystal packing analysis suggests that the LBD2 AF-2 is in close proximity to DBD1 of a crystallographic neighbor which likely precludes peptide binding.

The DBDs form a head-to-head dimer arrangement in the multidomain structure, which recapitulates the structure of the isolated GR DBDs on the same GBS (PDB: 3G9O) with a Cα root mean square deviation (r.m.s.d.) of 0.876 (138 atoms) (Extended Data Fig. 2a). To validate the LBD structures in the complex, we determined the structure of the isolated,

monomeric wild type (WT) GR LBD in complex with velsecorat [GR_{LBD}(Vel)] and PGC1$\alpha_{134-154}$ (Extended Data Table 1). The $GR_{\Delta N}$(Vel) LBD1 and LBD2 both exhibit the typical 3 layered α-helical sandwich fold and overlay on the GR_{LBD}(Vel) structure with a Cα r.m.s.d. of 0.480 and 0.549 for LBD1 (248 atoms) and LBD2 (248 atoms), respectively (Extended Data Fig. 2b, c), confirming that the LBD V571M, F602S and C628D mutants of the $GR_{\Delta N}$ construct have minimal impact on the GR LBD conformation. The additional S404A and N517D mutants of the $GR_{\Delta N}$ construct are located in unstructured regions adjacent to the DBDs and are unlikely to affect the structure.

In contrast to the electron microscopy structures of multi-domain nuclear hormone receptors[22,23], the X-ray structures[24-27] generally display a more compact arrangement with significant contacts in between the LBDs and DBDs. However, the domain arrangement among the X-ray structures varies dramatically and the structural overlay reveals that the GR organization is unique (Extended Data Fig. 7). The previous X-ray structures all bind to direct repeat DNA response elements with the DBDs arranged in a head-to-tail fashion in the quaternary complex. As the nucleotide linker length in between the binding sequences vary, the DBDs are placed on different sides along the DNA duplex. In addition, as for the other keto-steroid receptors, the isolated GR LBD is monomeric in solution, while the receptors with known multi-domain structures form stable head-to-head LBD-LBD dimers that are conserved in the multi-domain structures. Together, this presents distinct boundary conditions for positioning the LBDs in the quaternary complex. However, despite the differences in the domain arrangement, it is interesting to note that as observed for the previous structures[24-27], the LBD1 H9-H10 loop is part of the interface with the DBD on the 5' DNA binding sequence (DBD1).

The receptor transcriptional regulation is highly ligand dependent[28,29]. To investigate potential ligand impact on the domain arrangement, we determined the structure of $GR_{\Delta N}$ in complex with the steroid fluticasone furoate, the GBS from *SGK-1* and the PGC1α coregulator peptide [($GR_{\Delta N}$(FF)-*SGK*-PGC1α), Extended Data Table S1]. $GR_{\Delta N}$(FF)-*SGK*-PGC1α crystallizes in the same space group as $GR_{\Delta N}$(Vel)-*SGK*-PGC1α, and the structures of the individual domains are very similar with a Cα r.m.s.d. of 1.004 and 0.852 for LBD1 and LBD2 (248 atoms), respectively, and 0.340 for the DBDs (142 atoms, Fig. 4a).

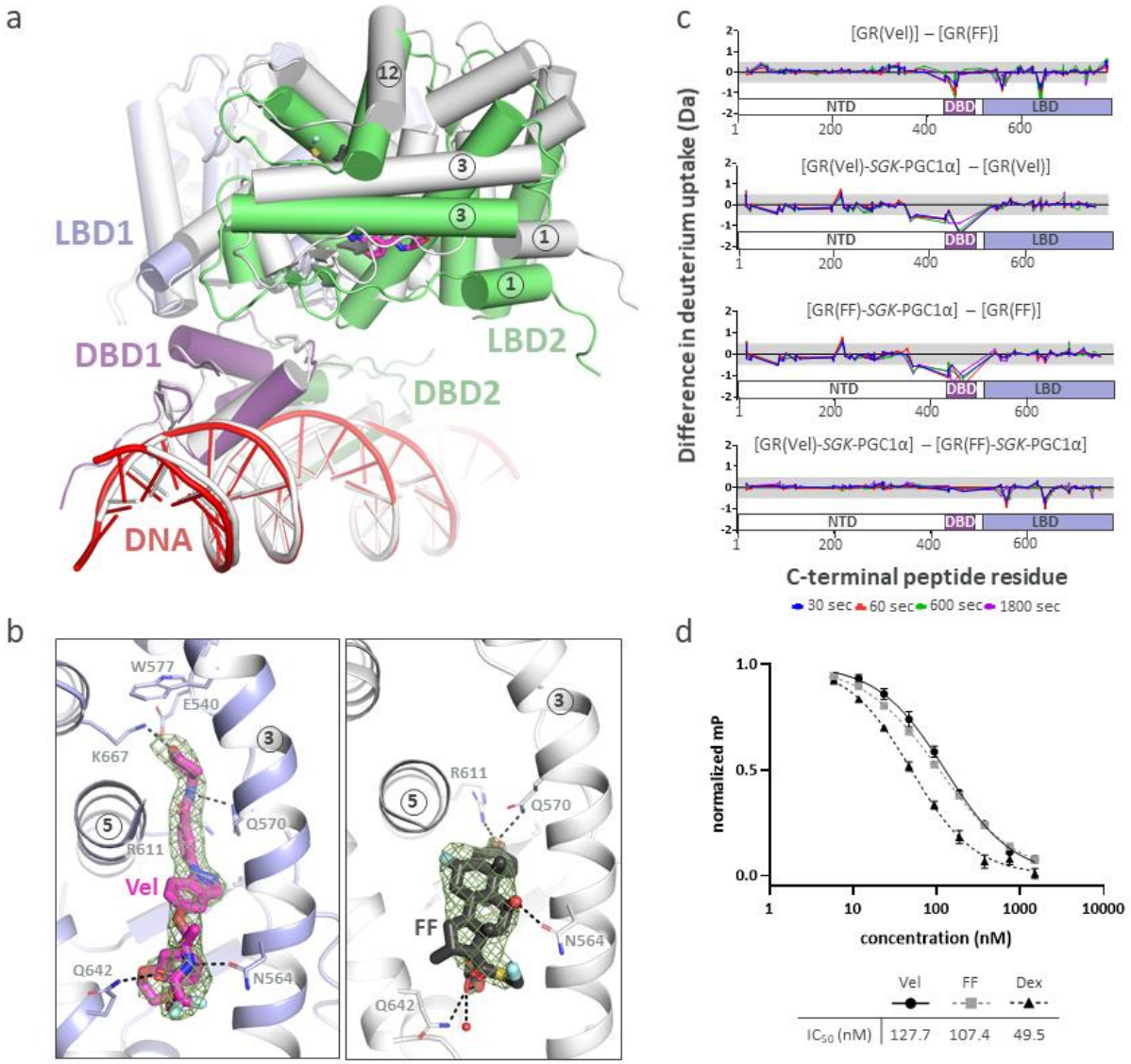

Figure 4 | Ligand specific structural rearrangements.

a, Overlay of the structures of $GR_{\Delta N}$-*SGK*-PGC1α complexes in the presence of velsecorat (in color) and FF (in white). The structures have been overlaid using the 5' GBS binding motif as reference. GR LBD helix numbering is annotated within the circles. **b,** Ligand binding site with velsecorat (magenta) and FF (dark gray). |*Fo*|-|*Fc*| densities (in green) were calculated before models were refined with ligands and are contoured at 3σ. **c,** HDX difference plots showing deuterium uptake difference [complex A] – [complex B] for all peptides captured from the full-length receptor. Negative values indicate that peptides are protected in A relative to B and vice versa. **d,** Competition binding experiments monitoring exchange of 6-FAM-*SGK* dsDNA in complex with GR(ligand) with unlabeled *SGK* dsDNA using fluorescence polarization. Data points are mean ± s.e.m. of three replicates from one experiment.

Velsecorat and fluticasone furoate both bind in the same central ligand binding pocket forming an interaction with N564, which is important for stabilizing H12 in the active position (Fig. 4b)[30]. As for $GR_{\Delta N}$(Vel), H12 is positioned in the active conformation in both $GR_{\Delta N}$(FF) LBDs, but the PGC1α peptide is only observed at the AF-2 site for LBD1. Opposite N564, both compounds form an interaction with Q642, but the position of the side-chain is different due to the less bulky, non-steroidal scaffold, of velsecorat. The most notable distinction, however, is beyond the intersect in between H3 and H5. While the 3-keto moiety of the steroid interacts with Q572 and R611, velsecorat rearranges these residues and extends into a novel pocket beneath W577, at the intersect in between H1, H3 and H5.

While the domain arrangement is conserved in the quaternary complexes, the position of LBD2 is slightly shifted in the $GR_{\Delta N}$(FF)-*SGK*-PGC1α structure (Fig. 4a). This is likely because fluticasone furoate has a bulkier substituent at the 17α position and pushes on the H6-H7 region in LBD1 (Extended Data Fig. 8). This region is part of the LBD-LBD dimer

interface and consequently shifts the position of the H10/11 in the other monomer. The H6-H7 region is known to be flexible and may be part of the ligand entry mechanism[31]. While fluticasone furoate also makes an analogous push on the H6-H7 region in LBD2, LBD1 is less likely to move since the H10/11 region interacts with DBD1. As a consequence, the $GR_{\Delta N}$(FF)-*SGK*-PGC1α LBD2 position is shifted, and the total buried surface areas are reduced to 704.5 $Å^2$ at the LBD dimer interface and to 16.6 $Å^2$ in between LBD2 and DBD1.

To investigate how these structural changes translate to receptor modulation in solution, we expressed the full-length receptor with velsecorat, fluticasone furoate or dexamethasone and performed hydrogen/deuterium exchange mass spectrometry (HDX-MS). The deuterium uptake over time correlates with solvent accessibility and protein dynamics[32]. Comparing GR(Vel) to GR(FF) (Fig. 4c, top panel [GR(Vel)]-[GR(FF)], and Extended Data Fig. 9), the data confirms that velsecorat protects the protein near helix 1 where the ligand extends into the novel pocket (residues 536-565) and the region near H6 and H7 where we observed the rearrangements in the $GR_{\Delta N}$(FF) structure (residues 621-647). Interestingly, the data revealed that velsecorat and fluticasone furoate also impact the deuterium uptake level in a region of the DBD differently, suggesting ligand specific communication across the two domains, even in absence of DNA.

When analyzing the complex of GR with *SGK* GBS and the PGC1α peptide with HDX-MS, we obtained a lower peptide coverage than for the GR protein alone (Extended Data Fig. 10). A large section of the DBD (residues 424-467), including the N-terminal α-helix 1, the dimerization loop (D-loop) and the lever arm, is protected from HDX in the GR(Vel)-*SGK*-PGC1α and GR(FF)-*SGK*-PGC1α complexes compared to the isolated GR(Vel) and GR(FF) samples, confirming DNA binding (Fig. 4c, second and third panel from top). However, when

comparing the HDX-MS data from the GR(Vel)-*SGK*-PGC1α and the GR(FF)-*SGK*-PGC1α complexes, we did not detect differences in the DBD domain (Fig. 4c, bottom panel). This may be due to DNA binding itself being such a dominant stabilization process engaging many residues at the interface that it obscures potential ligand specific rearrangements across the two domains. The HDX difference data for GR(Dex) supports that dexamethasone is of the same steroid chemotype as fluticasone furoate with no significant signal in the LBD (Extended Data Fig. 11, top panel). The GR(Dex) data also confirms ligand specific communication across the LBD-DBD domains in absence of DNA.

To further explore how the ligand pharmacophore impacts the DNA binding event, we used fluorescence polarization (FP) to analyze the stability of the GR(ligand) in complex with fluorescently labelled 6-FAM-*SGK* dsDNA, by adding increasing concentrations of competing unlabeled *SGK* and determined the IC_{50}. As the cytokine release inhibition assay highlighted (Fig. 1c), velsecorat and fluticasone furoate are the stronger GR agonists and they also lead to a 2-fold increase in the stability of the GR–*SGK* complex in comparison to dexamethasone, reflected by the higher concentration of unlabeled *SGK* required to exchange the labelled DNA (Fig. 3d). Altogether, the HDX-MS and FP data provide biophysical support for inter-domain communication that could form the basis for ligand driven functional differentiation.

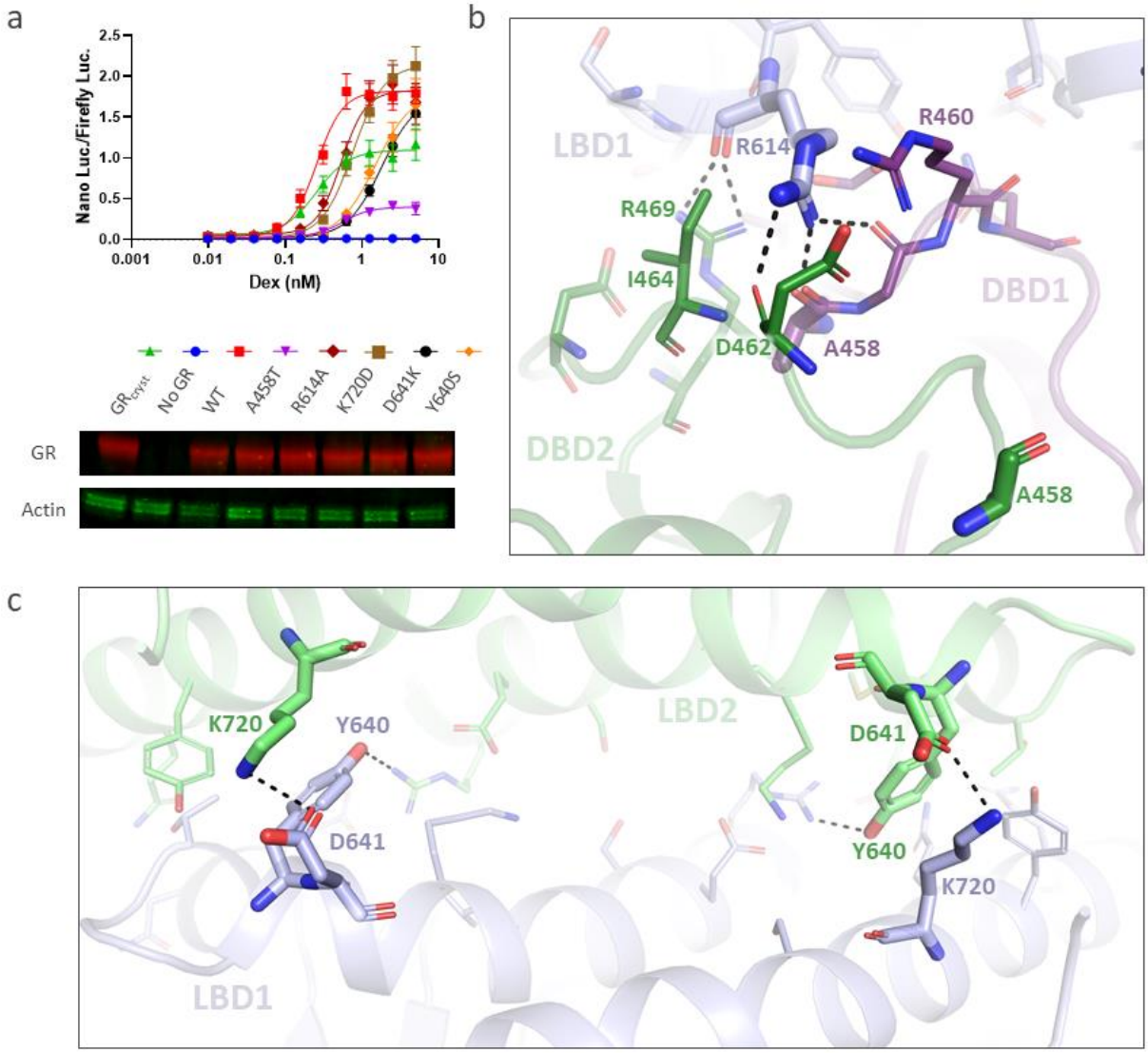

Figure 5 | Domain interfaces in the GR$_{\Delta N}$(Vel) complex. a, MMTV reporter assay using GR$_{cryst}$(S404A, N517D, V571M, F602S, C638D), GR$_{WT}$, GR(A458T), GR(R614A), GR(K720D), GR(D641K) and GR(Y640S). Data points are mean ± s.e.m. of eight replicates from four experiments. The corresponding western blots showing GR and actin protein expression levels in the bottom panel. **b,** Interface of LBD1 with DBD1 and DBD2 and **c,** LBD1-LBD2 interface in GR(Vel)-*SGK*-PGC1α. The residues mutated in the transcriptional activation studies (**a**) are highlighted in bold.

To explore the relevance of the receptor interfaces for the signaling complex, we designed FL GR constructs with mutants located in the domain junctions. We transfected the GR constructs and a luciferase reporter under the control of the mouse mammary tumor virus (MMTV) promoter into COS7 cells, which lack endogenous GR, to monitor receptor activation in response to increasing concentrations of dexamethasone. All GR protein constructs express well (Fig. 5a, bottom panels). WT GR activates the luciferase reporter in response to dexamethasone with an EC_{50} of 257 pM (Fig. 5a, top graph). The GR construct containing the crystallization mutations, GR_{cryst}, exhibits a similar EC_{50} of 252 pM confirming that mutants in the $GR_{\Delta N}$ construct have limited effect on signaling potency. However, the maximal signaling efficacy is reduced. The crystallization mutant construct is designed to stabilize the receptor in a specific state. It is conceivable that the signaling event requires structural dynamics that the mutations in GR_{cryst} interfere with. The control mutant A458T, which is located in the DBD D-loops (Fig. 5b) causing a clash in the DBD-DBD interface[33], lowers the EC_{50} to 555 pM accompanied by a reduction of the maximal signaling efficacy. In LBD1, R614 engages in H-bonds with residues in the D-loops of both DBD1 (G459, A458) and DBD2 (D462, R469) and exhibits hydrophobic contacts with I464 of DBD2 and R460 of DBD1 (Fig. 5b). In keeping with this central position, the R614A mutant shifts the signaling EC_{50} to 533 pM. At the LBD1-LBD2 interface, we designed the Y640S, D641K and K720D mutant constructs (Fig. 5c), yielding a change in the signaling potency to an EC_{50} of 1.50 nM, 1.79 nM and 762 pM, respectively. In humans, the D641V mutant has been reported to be associated with glucocorticoid resistance[34]. Altogether, the functional data presented here confirm that the strategically placed mutants impair receptor signaling. However, a full characterization of the receptor interfaces requires a comprehensive functional study with mutants distributed across all receptor surfaces.

70 years ago Phillip Hench administered the hormone cortisone to patients with rheumatoid arthritis with a transformative outcome[35]. After the isolation of human and rat receptors[36,37] and identification of the GR cDNA[38,39], GR remains one of the most intensely studied nuclear receptors. GR is distinct among the steroid receptors in that it binds a wider range of DNA elements, either as a dimer or as a monomer[40]. As such, the individual receptor domains are required to adapt to different oligomeric arrangements. The structures of $GR_{\Delta N}$ binding to the canonical GBS reveal a distinct domain arrangement. The keto-steroid receptor specific C-terminal extension prevents the formation of the strong LBD dimer observed in ER[16]. Instead, the GR LBD dimerization surface is shifted to an adjacent overlapping position, and the LBDs form a unique head-to-tail dimer with a relatively small interface. We propose that this may be a consequence of the requirement to signal in different contexts, as a strong LBD dimer would potentially shift the signaling balance. The detailed quaternary arrangement presented here provides a structural context for disease mutations and the information on the domain interfaces will provide critical insights for future drug design. Future studies of multidomain GR constructs in complex with DNA half-sites, inverted repeat binding elements and different coregulators will further build the understanding of how the signaling flexibility correlates with different structural arrangements.

References

1 Eick, G. N. & Thornton, J. W. Evolution of steroid receptors from an estrogen-sensitive ancestral receptor. *Molecular and Cellular Endocrinology* **334**, 31-38, doi:10.1016/j.mce.2010.09.003 (2011).

2 Weikum, E. R., Knuesel, M. T., Ortlund, E. A. & Yamamoto, K. R. Glucocorticoid receptor control of transcription: precision and plasticity via allostery. *Nature Reviews Molecular Cell Biology* **18**, 159, doi:10.1038/nrm.2016.152 (2017).

3 Meijsing, S. H. *et al.* DNA Binding Site Sequence Directs Glucocorticoid Receptor Structure and Activity. *Science* **324**, 407-410, doi:10.1126/science.1164265 (2009).

4 Schiller, B. J., Chodankar, R., Watson, L. C., Stallcup, M. R. & Yamamoto, K. R. Glucocorticoid receptor binds half sites as a monomer and regulates specific target genes. *Genome Biology* **15**, 418, doi:10.1186/s13059-014-0418-y (2014).

5 Hudson, W. H., Youn, C. & Ortlund, E. A. The structural basis of direct glucocorticoid-mediated transrepression. *Nature Structural & Molecular Biology* **20**, 53, doi:10.1038/nsmb.2456 (2012).

6 Watson, L. C. *et al.* The glucocorticoid receptor dimer interface allosterically transmits sequence-specific DNA signals. *Nature Structural & Molecular Biology* **20**, 876, doi:10.1038/nsmb.2595 (2013).

7 Veleiro, A. S., Alvarez, L. D., Eduardo, S. L. & Burton, G. Structure of the Glucocorticoid Receptor, a Flexible Protein That Can Adapt to Different Ligands. *ChemMedChem* **5**, 649-659, doi:10.1002/cmdc.201000014 (2010).

8 Hemmerling, M. *et al.* Selective Nonsteroidal Glucocorticoid Receptor Modulators for the Inhaled Treatment of Pulmonary Diseases. *Journal of Medicinal Chemistry* **60**, 8591-8605, doi:10.1021/acs.jmedchem.7b01215 (2017).

9 Biggadike, K. *et al.* X-ray Crystal Structure of the Novel Enhanced-Affinity Glucocorticoid Agonist Fluticasone Furoate in the Glucocorticoid Receptor−Ligand Binding Domain. *Journal of Medicinal Chemistry* **51**, 3349-3352, doi:10.1021/jm800279t (2008).

10 Brown, M. N. *et al.* Efficacy and safety of AZD7594, an inhaled non-steroidal selective glucocorticoid receptor modulator, in patients with asthma: a phase 2a randomized, double blind, placebo-controlled crossover trial. *Respiratory Research* **20**, 37, doi:10.1186/s12931-019-1000-7 (2019).

11 Shefrin, A. E. & Goldman, R. D. Use of dexamethasone and prednisone in acute asthma exacerbations in pediatric patients. *Can Fam Physician* **55**, 704-706 (2009).

12 Syed, Y. Y. Fluticasone Furoate/Vilanterol: a Review of Its Use in Patients with Asthma. *Drugs* **75**, 407-418, doi:10.1007/s40265-015-0354-5 (2015).

13 Grasso, E. M., Majumdar, A., Wrabl, J. O., Frueh, D. P. & Hilser, V. J. Conserved allosteric ensembles in disordered proteins using TROSY/anti-TROSY R2-filtered spectroscopy. *Biophysical Journal* **120**, 2498-2510, doi:10.1016/j.bpj.2021.04.017 (2021).

14 Shiau, A. K. *et al.* The Structural Basis of Estrogen Receptor/Coactivator Recognition and the Antagonism of This Interaction by Tamoxifen. *Cell* **95**, 927-937, doi:10.1016/S0092-8674(00)81717-1 (1998).

15 Köhler, C. *et al.* Dynamic allosteric communication pathway directing differential activation of the glucocorticoid receptor. *Science Advances* **6**, eabb5277, doi:10.1126/sciadv.abb5277 (2020).

16 Hochberg, G. K. A. *et al.* A hydrophobic ratchet entrenches molecular complexes. *Nature* **588**, 503-508, doi:10.1038/s41586-020-3021-2 (2020).

17 Bianchetti, L. *et al.* Alternative dimerization interfaces in the glucocorticoid receptor-α ligand binding domain. *Biochimica et Biophysica Acta (BBA) - General Subjects* **1862**, 1810-1825, doi:10.1016/j.bbagen.2018.04.022 (2018).

18 Robblee, J. P., Miura, M. T. & Bain, D. L. Glucocorticoid Receptor–Promoter Interactions: Energetic Dissection Suggests a Framework for the Specificity of Steroid Receptor-Mediated Gene Regulation. *Biochemistry* **51**, 4463-4472, doi:10.1021/bi3003956 (2012).

19 Bledsoe, R. K. *et al.* Crystal Structure of the Glucocorticoid Receptor Ligand Binding Domain Reveals a Novel Mode of Receptor Dimerization and Coactivator Recognition. *Cell* **110**, 93-105, doi:10.1016/S0092-8674(02)00817-6 (2002).

20 Paakinaho, V., Johnson, T. A., Presman, D. M. & Hager, G. L. Glucocorticoid receptor quaternary structure drives chromatin occupancy and transcriptional outcome. *Genome Research* (2019).

21 Presman, D. M. & Hager, G. L. More than meets the dimer: What is the quaternary structure of the glucocorticoid receptor? *Transcription* **8**, 32-39, doi:10.1080/21541264.2016.1249045 (2017).

22 Maletta, M. *et al.* The palindromic DNA-bound USP/EcR nuclear receptor adopts an asymmetric organization with allosteric domain positioning. *Nature Communications* **5**, 4139, doi:10.1038/ncomms5139 (2014).

23 Orlov, I., Rochel, N., Moras, D. & Klaholz, B. P. Structure of the full human RXR/VDR nuclear receptor heterodimer complex with its DR3 target DNA. *The EMBO Journal* **31**, 291-300, doi:10.1038/emboj.2011.445 (2012).

24 Chandra, V. *et al.* Structure of the intact PPAR-γ–RXR-α nuclear receptor complex on DNA. *Nature* **456**, 350, doi:10.1038/nature07413 (2008).

25 Chandra, V. *et al.* Multidomain integration in the structure of the HNF-4α nuclear receptor complex. *Nature* **495**, 394, doi:10.1038/nature11966 (2013).

26 Chandra, V. *et al.* The quaternary architecture of RARβ–RXRα heterodimer facilitates domain–domain signal transmission. *Nature Communications* **8**, 868, doi:10.1038/s41467-017-00981-y (2017).

27 Lou, X. *et al.* Structure of the retinoid X receptor α–liver X receptor β (RXRα–LXRβ) heterodimer on DNA. *Nature Structural & Molecular Biology* **21**, 277-281, doi:10.1038/nsmb.2778 (2014).

28 Hegelund Myrbäck, T. *et al.* Effects of a selective glucocorticoid receptor modulator (AZD9567) versus prednisolone in healthy volunteers: two phase 1, single-blind, randomised controlled trials. *The Lancet Rheumatology* **2**, e31-e41, doi:10.1016/S2665-9913(19)30103-1 (2020).

29 Ripa, L. *et al.* Discovery of a Novel Oral Glucocorticoid Receptor Modulator (AZD9567) with Improved Side Effect Profile. *Journal of Medicinal Chemistry* **61**, 1785-1799, doi:10.1021/acs.jmedchem.7b01690 (2018).

30 Liu, X. *et al.* Disruption of a key ligand-H-bond network drives dissociative properties in vamorolone for Duchenne muscular dystrophy treatment. *Proceedings of the National Academy of Sciences* **117**, 24285-24293, doi:10.1073/pnas.2006890117 (2020).

31 Edman, K. *et al.* Ligand Binding Mechanism in Steroid Receptors: From Conserved Plasticity to Differential Evolutionary Constraints. *Structure (London, England : 1993)* **23**, 2280-2290, doi:10.1016/j.str.2015.09.012 (2015).

32 in *Hydrogen Exchange Mass Spectrometry of Proteins: Fundamentals, Methods, and Applications* (ed David D. Weis) (2016).

33 Heck, S. *et al.* A distinct modulating domain in glucocorticoid receptor monomers in the repression of activity of the transcription factor AP-1. *The EMBO Journal* **13**, 4087-4095, doi:10.1002/j.1460-2075.1994.tb06726.x (1994).

34 Hurley, D. M. *et al.* Point mutation causing a single amino acid substitution in the hormone binding domain of the glucocorticoid receptor in familial glucocorticoid resistance. *The Journal of Clinical Investigation* **87**, 680-686, doi:10.1172/JCI115046 (1991).

35 Benedek, T. G. History of the development of corticosteroid therapy. *Clinical and experimental rheumatology* **29**, S-5-12 (2011).

36 Gehring, U. & Hotz, A. Photoaffinity labeling and partial proteolysis of wild-type and variant glucocorticoid receptors. *Biochemistry* **22**, 4013-4018, doi:10.1021/bi00286a004 (1983).

37 Simons, S. S., Jr. & Thompson, E. B. Dexamethasone 21-mesylate: an affinity label of glucocorticoid receptors from rat hepatoma tissue culture cells. *Proceedings of the National Academy of Sciences* **78**, 3541-3545, doi:10.1073/pnas.78.6.3541 (1981).

38 Hollenberg, S. M. *et al.* Primary structure and expression of a functional human glucocorticoid receptor cDNA. *Nature* **318**, 635-641, doi:10.1038/318635a0 (1985).

39 Miesfeld, R. *et al.* Genetic complementation of a glucocorticoid receptor deficiency by expression of cloned receptor cDNA. *Cell* **46**, 389-399, doi:10.1016/0092-8674(86)90659-8 (1986).

40 Hudson, W. H. *et al.* Distal substitutions drive divergent DNA specificity among paralogous transcription factors through subdivision of conformational space. *Proceedings of the National Academy of Sciences* **113**, 326-331, doi:10.1073/pnas.1518960113 (2016).

a

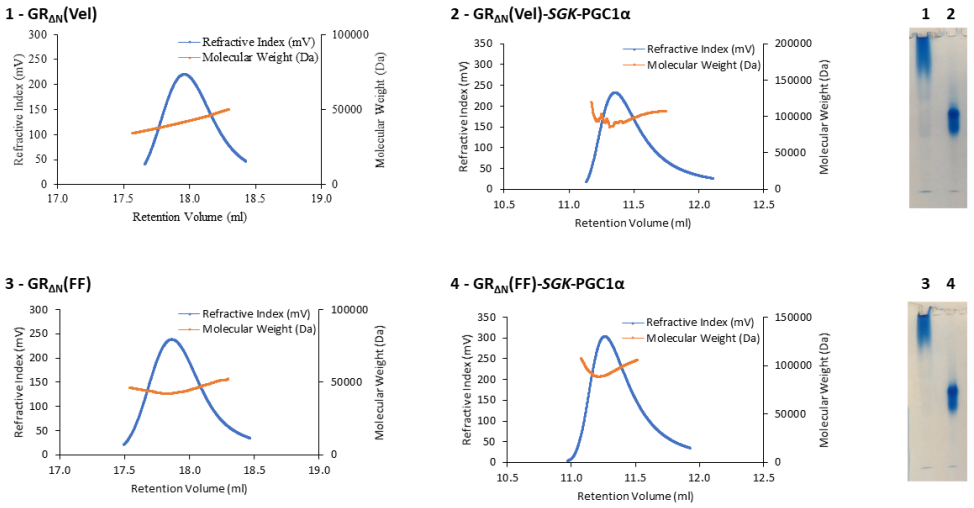

c

b

Sample No	Sample	Protein	Peptide	dsDNA	Ligand	MALS MW (kDa)	calculated MW (kDa)
1	GR$_{\Delta N}$(Vel)	GR$_{385-777}$[S404A, N517D, V571M, F602S, C638D]			velsecorat	43.14	44.5
2	GR$_{\Delta N}$(Vel)-*SGK*-PGC1α	GR$_{385-777}$[S404A, N517D, V571M, F602S, C638D]	PGC1α	*SGK*23blunt	velsecorat	98.14	107.5
3	GR$_{\Delta N}$(FF)	GR$_{385-777}$[S404A, N517D, V571M, F602S, C638D]			fluticasone furoate	45.15	44.5
4	GR$_{\Delta N}$(FF)-*SGK*-PGC1α	GR$_{385-777}$[S404A, N517D, V571M, F602S, C638D]	PGC1α	*SGK*23overhang	fluticasone furoate	98.47	107.5

Extended Data Figure 1 | SEC-MALS of GR$_{\Delta N}$(Vel), GR$_{\Delta N}$(FF), GR$_{\Delta N}$(Vel)-SGK-PGC1α and GR$_{\Delta N}$(FF)-SGK-PGC1α. a, The monomeric GR proteins and dimeric GR complexes eluted as single peaks. **b,** The experimentally determined and expected molecular weights. **c,** GR proteins and GR complexes separated on a native PAGE.

Extended Data Table 1 | Crystallographic data collection and refinement statistics.

Name	$GR_{\Delta N}$(Vel)-*SGK*-PGC1α	GR_{LBD}(Vel)-PGC1α	$GR_{\Delta N}$(FF)-*SGK*-PGC1α
GR construct	$GR\alpha_{385-777}$ [S404A, N517D, V571M, F602S, C638D]	$GR\alpha_{529-777}$ [WT]	$GR\alpha_{385-777}$ [S404A, N517D, V571M, F602S, C638D]
Ligand	Velsecorat	Velsecorat	fluticasone furoate
peptide	$PGC1\alpha_{134-154}$	$PGC1\alpha_{134-154}$	$PGC1\alpha_{134-154}$
DNA	*SGK*23blunt	**N/A**	*SGK*23overhang
Data collection			
Space group	P212121	P21	P212121
a, b, c (Å)	80.21, 122.72, 130.45	42.34, 73.43, 43.93	79.67, 119.72, 135.53
α, β, ɣ (°)	90.0, 90.0, 90.0	90.0, 105.86, 90.0	90.0, 90.0, 90.0
Wavelength (Å)	0.96550	0.97242	0.96545
Resolution (Å)	89.39-2.5 (2.87-2.5)	73.43-2.2 (2.27-2.2)	68.7-2.7 (3.0-2.7)
Rmerge	0.082 (0.792)	0.124 (0.928)	0.067 (1.035)
Rpim	0.036 (0.373)	0.081 (0.466)	0.029 (0.425)
I/σ(I)	12.6 (1.9)	6.6 (1.7)	16.3 (1.6)
CC1/2 (%)	0.999 (0.744)	0.995 (0.709)	0.999 (0.706)
Completeness spherical (%)	51.0 (7.6)		70.2 (13.8)
Completeness ellipsoidal (%)	93.4 (76.1)		93.9 (63.5)
Completeness		99.0 (88.1)	
Multiplicity (%)	6.3 (5.4)	3.3 (3.1)	6.5 (6.9)
Refinement			
Resolution (Å)	89.39-2.5	42.26-2.2	68.7-2.7
Total reflections	45176	42980	36333
Unique reflections	23070	13075	24963
Rwork/Rfree (%)	0.202/0.263	0.226/0.281	0.216/0.254
No. of non-hydrogen atoms			
Protein	5299	2168	5262
Nucleic Acid	939	-	896
Ligands	116	44	90
Water	64	46	30
Average B-factor ($Å^2$)	88.0	50.0	103.0
Wilson B-factor ($Å^2$)	66.0	27.7	76.1
RMS deviations			
Bond lengths (Å)	0.008	0.008	0.008
Bond angles (°)	0.92	0.97	0.92
Ramachandran			
Most favored (%)	94	98	94
Outliers (%)	0	0	1
Clashscore	5	2	6
PDB code	7PRW	7PRX	7PRV

Values in parentheses are for the highest resolution shell.

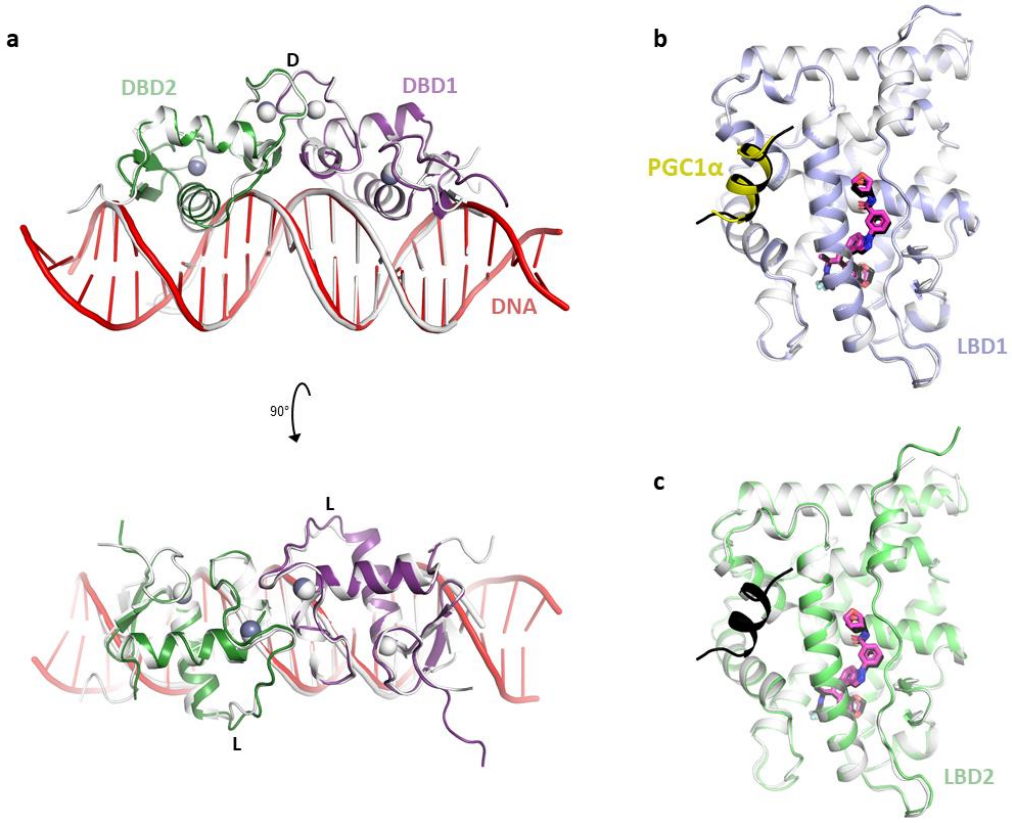

Extended Data Figure 2 | GR$_{\Delta N}$(Vel)-*SGK*-PGC1α domains overlaid on structures of the isolated domains. a, DBD1 (purple), DBD2 (green) and dsDNA (red) overlaid on the structure of the DBD dimer alone on the same GBS (PDB: 3G9O, all in white). Zn atoms are denoted as grey and white spheres, respectively. **b,** LBD1 (blue) with velsecorat (magenta) and coactivator peptide PGC1α$_{134\text{-}154}$ (yellow) overlaid on the structure of GR$_{LBD}$ (white) in complex with velsecorat (black) and coactivator peptide PGC1α$_{134\text{-}154}$ (black). **c,** LBD2 (green) with velsecorat (magenta) overlayed on the structure of GR$_{LBD}$ (white) in complex with velsecorat (black) and coactivator peptide PGC1α$_{134\text{-}154}$ (black).

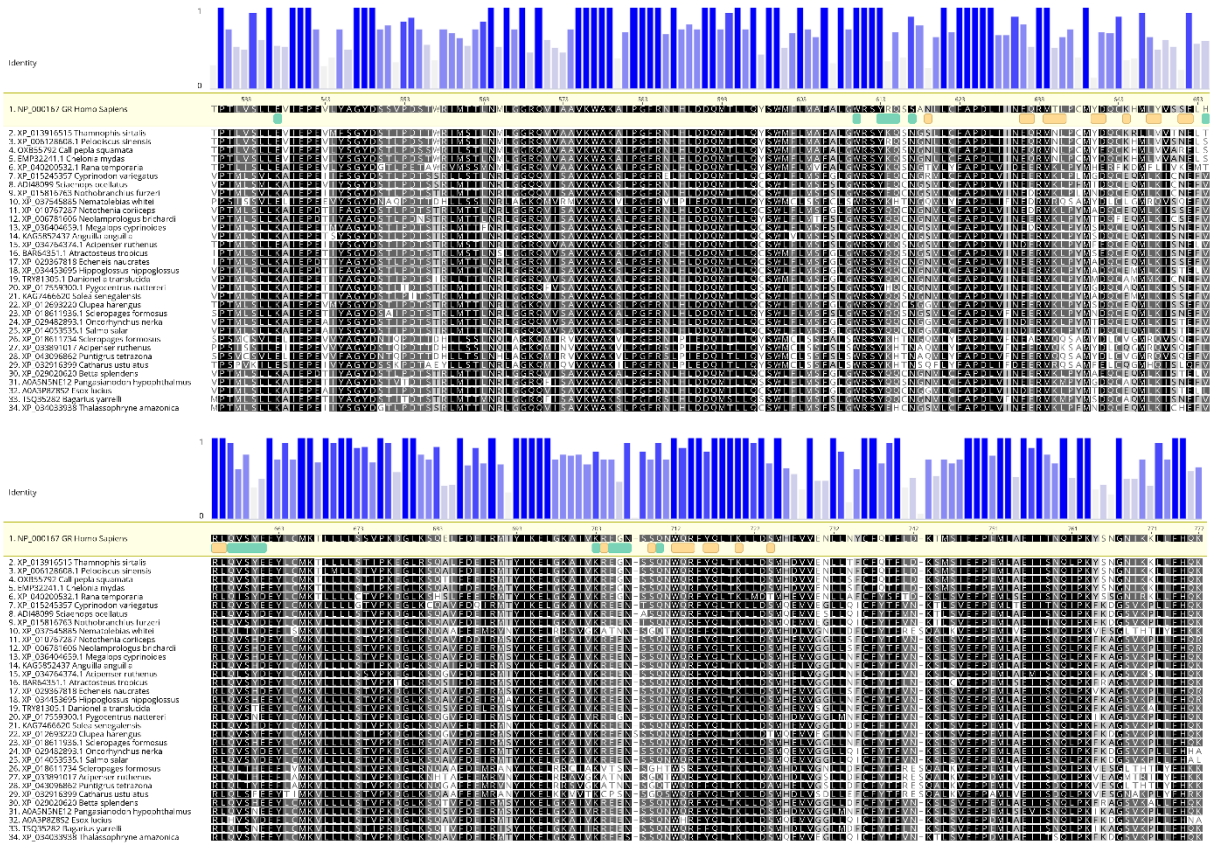

Extended Data Figure 3 | Sequence conservation of the GR LBD. Alignment of a set of diverse GR related vertebrate sequences with a pairwise identity of 37-84%. The mean pairwise column identity of each residue as calculated by Geneious Prime is shown as bars in the top graph. The residues involved in the LBD:LBD and LBD:DBD interfaces are indicated by orange and green boxes, respectively.

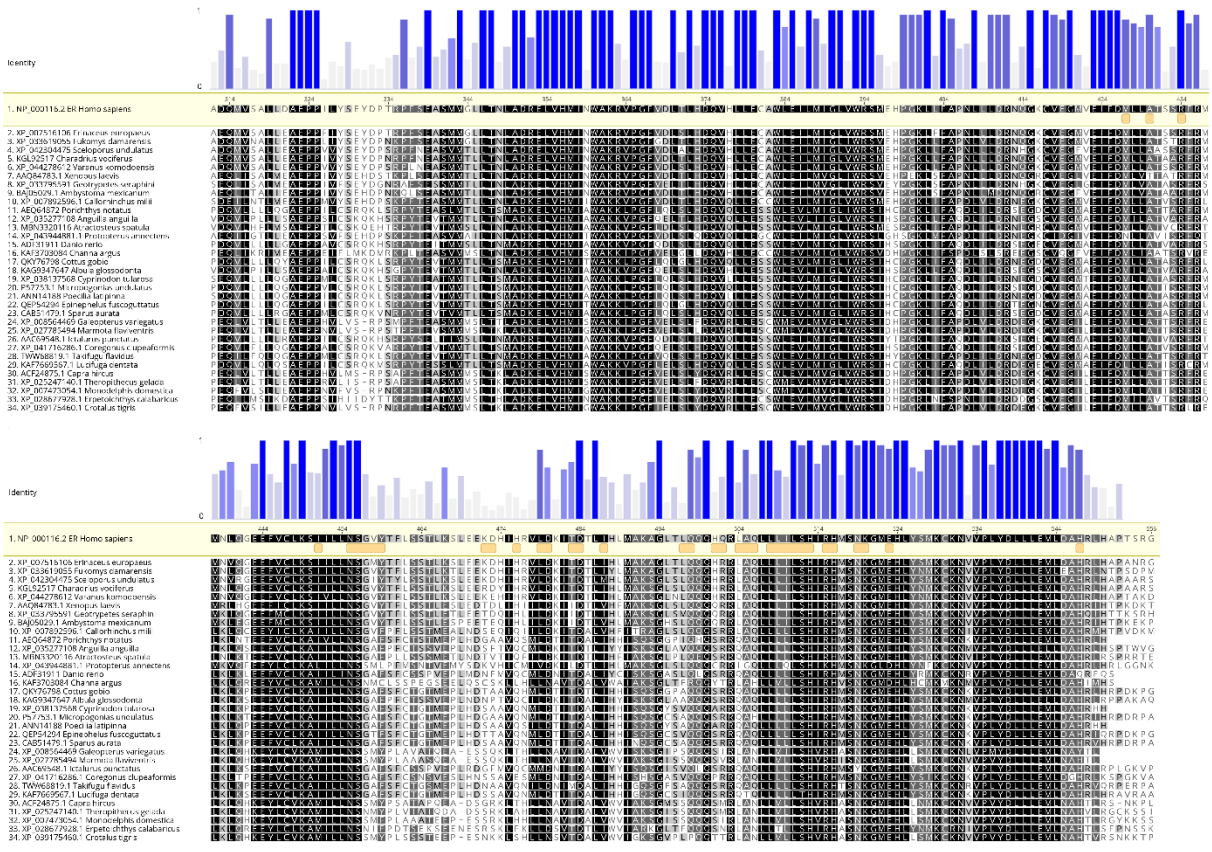

Extended Data Figure 4 | Sequence conservation of the ER LBD. a, Alignment of a set of diverse ER related vertebrate sequences with a pairwise identity of 38-90%. The mean pairwise column identity of each residue as calculated by Geneious Prime is shown as bars in the top graph. LBD dimer interface residues are highlighted with orange boxes.

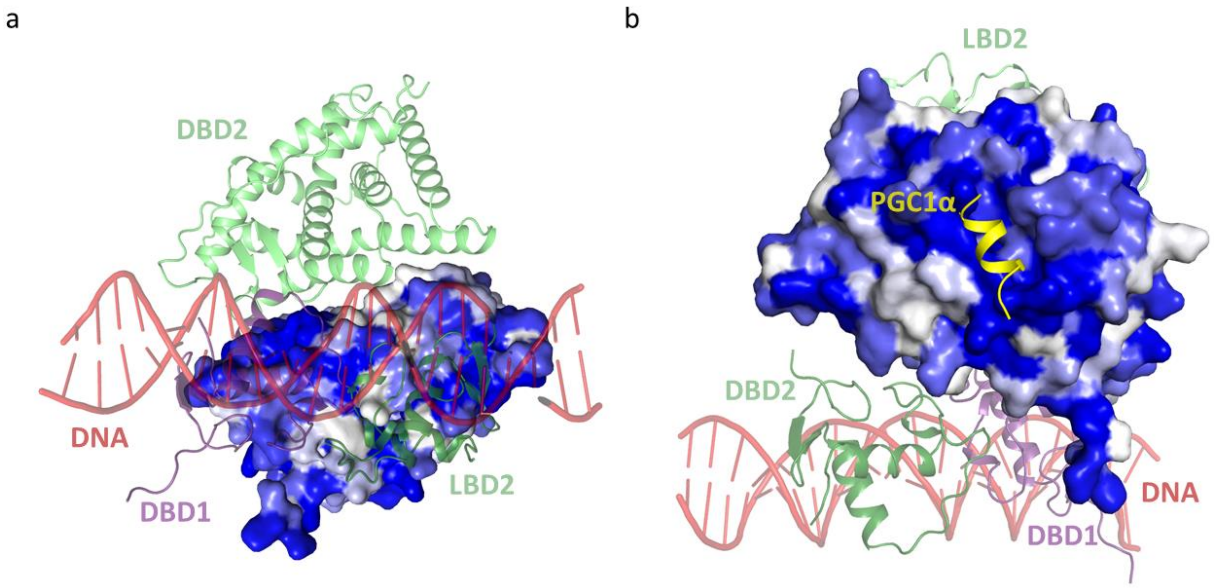

Extended Data Fig. 5 | Sequence conservation of key interfaces in the GR$_{\Delta N}$(Vel)-*SGK*-PGC1α complex. Conservation of GR LBD1 residues colored according to column identity between 0.4 (white) and 1.0 (blue) and shown as cartoon highlighting the LBD1 interface with **a,** the DBD and DNA and **b,** the PGC1α peptide (yellow).

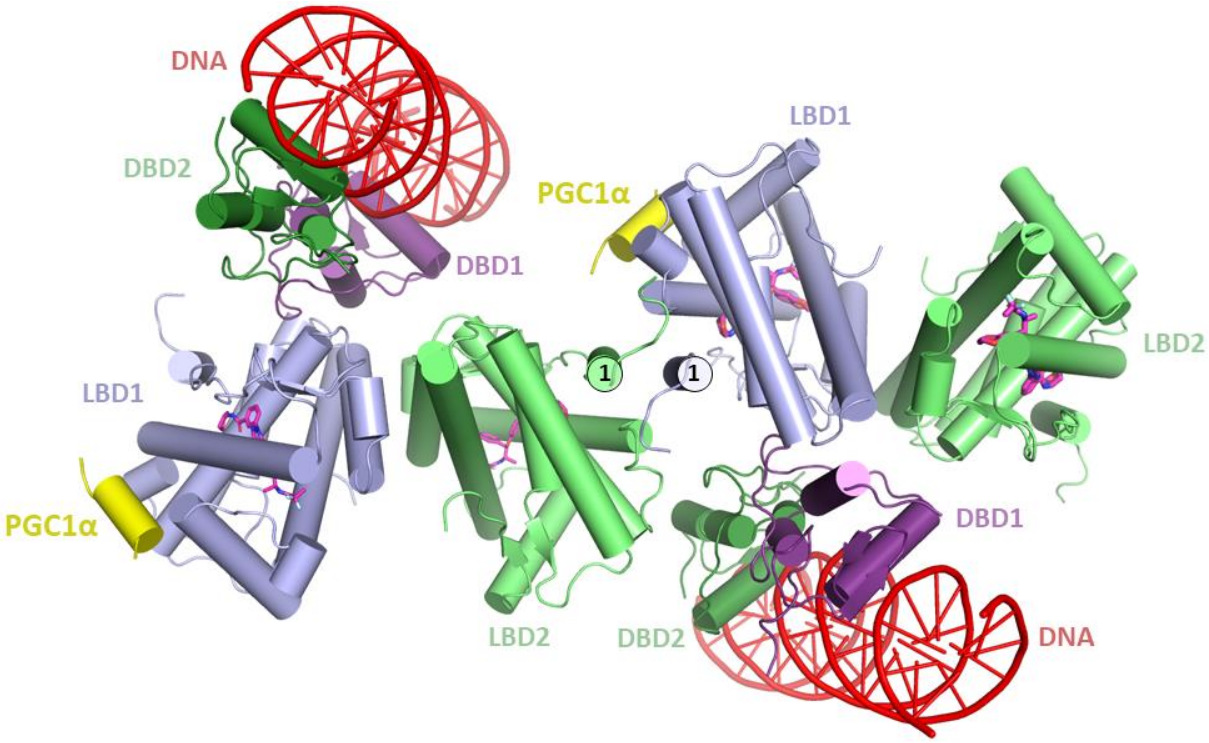

525

526

527 **Extended Data Fig. 6 | Structure of $GR_{\Delta N}$(Vel) in complex with *SGK* and PGC1α$_{134-154}$.**

528 The structure of $GR_{\Delta N}$(Vel)-*SGK*-PGC1α and a crystallographic neighbor highlighting

529 putative tetramer formation through the H1 interface.

530

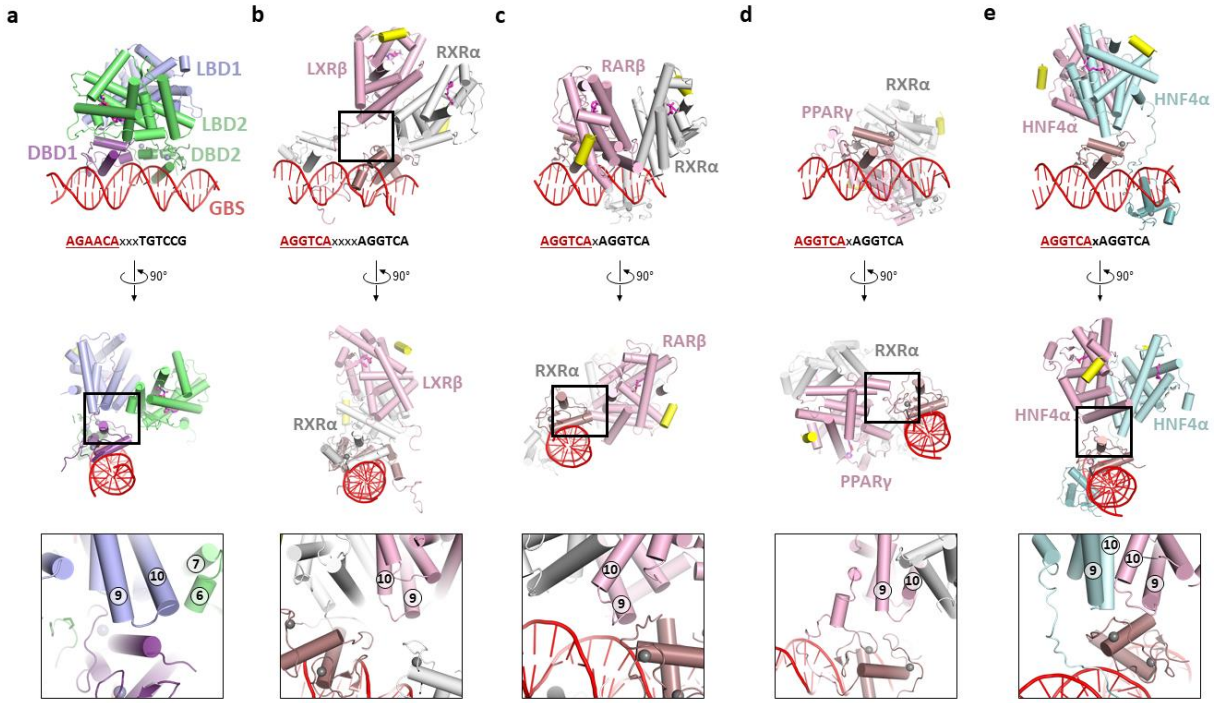

Extended Data Figure 7 | The domain organization of the multidomain nuclear receptor X-ray structures on DNA. a, $GR_{\Delta N}$(Vel)-*SGK*-PGC1α. **b,** LXRβ-RXRα **c,** RARβ-RXRα. **d,** PPARγ-RXRα. **e,** HNF-4α. The sequence of the DNA binding motif is indicated below the DNA duplex with x denoting nucleotide spacer. The structures have been overlaid using the 5' DNA binding sequence as reference (highlighted in red) and are all shown from the same angle. The different coregulator peptides are shown in yellow and the ligands in magenta.

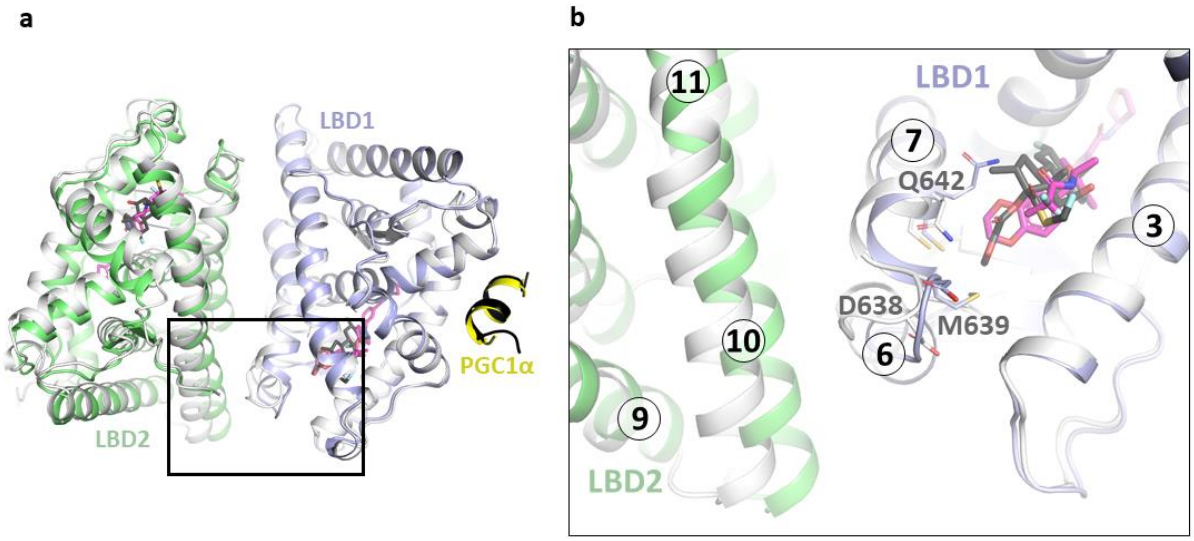

Extended Data Figure 8 | Fluticasone furoate rearranges the region where H6 and H7 meet. a, Overlay of the $GR_{\Delta N}$(FF)-*SGK*-PGC1α LBD1 (white) with PGC1α peptide in black on the $GR_{\Delta N}$(Vel)-*SGK*-PGC1α LBD1 (blue) with PGC1α peptide in yellow. Fluticasone furoate and velsecorat are shown in black and magenta, respectively. **b**, Fluticasone furoate repositions Q642 and pushes on D638 and M639, rearranging the H6-H7 loop. Helix numbering is annotated within the circles.

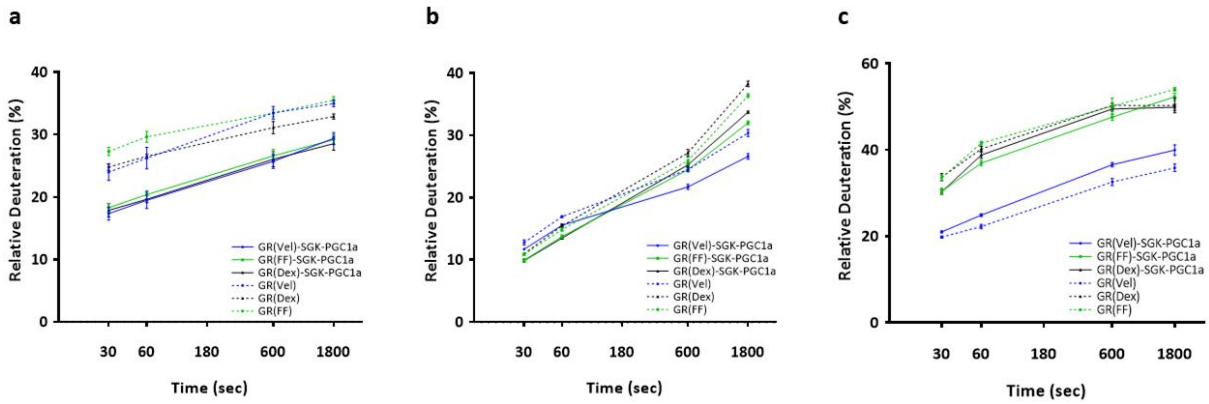

Extended Data Figure 9 | Relative deuteration of specific peptides in GR(Vel)-*SGK*-PGC1*α*, GR(FF)-*SGK*-PGC1*α*, GR(Dex)-*SGK*-PGC1*α*, GR(Vel), GR(FF) and GR(Dex) complexes. a, peptide 425-436. **b**, peptide 536-544. **c**, peptide 628-636.

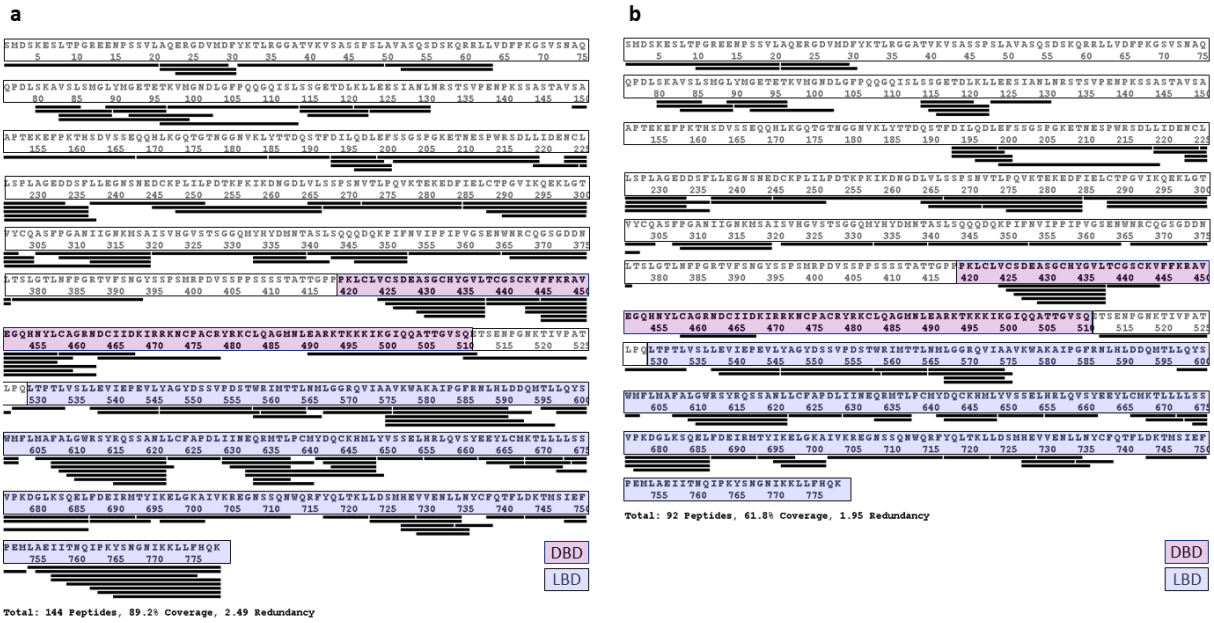

Extended Data Figure 10 | Protein coverage of GR and GR-*SGK*-PGC1α in HDX-MS. a, peptides used for HDX-MS analysis of GR. A coverage of 89.2% of the sequence was achieved. **b,** peptides used for HDX-MS analysis of GR-*SGK*-PGC1α complexes. A coverage of 61.8% of the sequence was achieved.

Extended Data Table 2 | Relative Uptake and Relative Uptake Error as identified with the DynamX 3.0 software (Waters) for all peptides and used for HDX analysis of GR in the presence of the ligands dexamethasone GR(Dex), fluticasone furoate GR(FF) and velsecorat GR(Vel).

Extended data table 2.docx

Extended Data Table 3 | Relative Uptake and Relative Uptake Error as identified with the DynamX 3.0 software (Waters) for all peptides and used for HDX analysis of GR(Dex), GR(FF), GR(Vel) and the complexes GR(Vel)-*SGK*-PGC1α, GR(FF)-*SGK*-

PGC1α and GR(Dex)-*SGK*-PGC1α. Vel=velsecorat, FF=fluticasone furoate, Dex=dexamethasone.

Extended data table 3.docx

Extended Data Table 4 | Relative Uptake Difference as identified with the DynamX 3.0 software (Waters) and p-values for all peptides used for HDX analysis of [GR(Vel)] minus [GR(FF)]. Significant p-values are highlighted in grey. Vel=velsecorat, FF=fluticasone furoate.

Extended data table 4.docx

Extended Data Table 5 | Relative Uptake Difference as identified with the DynamX 3.0 software (Waters) and p-values for all peptides used for HDX analysis of [GR(Vel)-*SGK*-PGC1α] minus [GR(FF)-*SGK*-PGC1α], [GR(Vel)-*SGK*-PGC1α] minus [GR(Vel)] and [GR(FF)-*SGK*-PGC1α] minus [GR(FF)]. Significant p-values are highlighted in grey. Vel=velsecorat, FF=fluticasone furoate.

Extended data table 5.docx

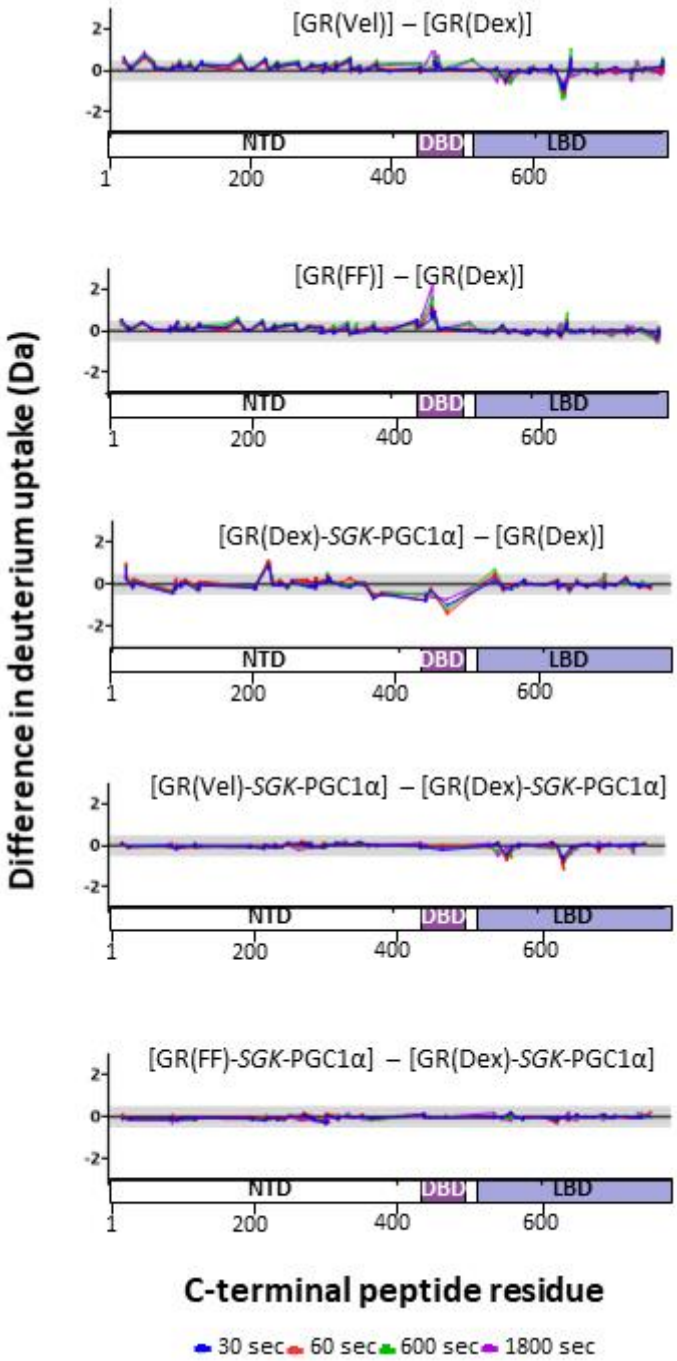

Extended Data Figure 11 | HDX difference plots showing deuterium uptake difference between [complex A] – [complex B] for all peptides. Negative value indicate that peptides are protected in A relative to B and vice versa.

Extended Data Table 6 | Relative Uptake Difference as identified with the DynamX 3.0 software (Waters) and p-values for all peptides used for HDX analysis of [GR(Vel)] minus [GR(Dex)] and [GR(FF)] minus [GR(Dex)]. Significant p-values are highlighted in grey. Vel=velsecorat, FF=fluticasone furoate, Dex=dexamethasone.

Extended data table 6.docx

Extended Data Table 7 | Relative Uptake Difference as identified with the DynamX 3.0 software (Waters) and p-values for all peptides used for HDX analysis of [GR(Dex)-*SGK*-PGC1α] minus [GR(Dex)], [GR(Vel)-*SGK*-PGC1α] minus [GR(Dex)-*SGK*-PGC1α] and [GR(FF)-*SGK*-PGC1α] minus [GR(Dex)-*SGK*-PGC1α]. Significant p-values are highlighted in grey. Vel=velsecorat, FF=fluticasone furoate, Dex=dexamethasone.

Extended data table 7.docx

Materials and Methods

Protein expression and purification

Optimized DNA sequences of GR (human $GR\alpha_{1\text{-}777}$ [WT]) and $GR_{\Delta N}$ (human $GR\alpha_{385\text{-}777}$ [S404A, N517D, V571M, F602S, C638D]) with N-terminal 6xHN-tag followed by a TEV site were cloned into pFastBac™1 and recombinant baculoviruses generated using the Bac-to-Bac® system (invitrogen). S404 is a known phosphorylation site[1] and the mutations N517D, V571M, F602S and C638D stabilize the GR LBD[2-4]. *Spodoptera frugiperda* insect cells (SF21) were cultured at 27°C in Gibco™ Sf-900™ II SFM medium and infected with baculovirus at a density of 2.5-3.0 x 10^6 mL^{-1}. 24 h after transfection 10 µM ligand in DMSO (velsecorat, fluticasone furoate or dexamethasone) was added to the cultures and 48 h after transfection the cells were harvested. The cells were resuspended in 20 mM Hepes pH 7.0, 10 % (v/v) glycerol, 1 mM TCEP, 10 µM ligand, cOmplete™ EDTA-free protease inhibitor cocktail (Roche, 1 tablet per 50 ml of solution) and flash frozen in liquid nitrogen. After thawing the NaCl concentration was adjusted to 0.5 M by adding adequate amounts of a stock solution containing 4.5 M NaCl, 20 mM Hepes pH 7.0, 10 % (v/v) glycerol, 1 mM TCEP, 10 µM ligand, the solution incubated for 15 Min on ice and the supernatant cleared by centrifuging at 30.000 g for 45 Min. The supernatant was incubated with WorkBeads™ 40 Ni-NTA (Bio-Works) for 2 hours at 4°C, the beads were washed by gravity flow with buffer containing 20 mM HEPES pH 7.0, 500 mM NaCl, 10 % glycerol, 1 mM TCEP, 10 µM ligand, 25 mM Imidazole and 5 mM ATP and the protein eluted with increasing Imidazole concentrations. The elution buffer was exchanged on a desalting column to 20 mM HEPES pH 7.0, 500 mM NaCl, 10 % glycerol, 1 mM TCEP, 10 µM ligand before the HN-tag was cleaved off by TEV digestion overnight at 4°C. The proteins were further purified by size

exclusion and the peak fractions pooled, concentrated to 1-3 mg/mL, flash frozen in liquid N_2 and stored at -80°C.

The wildtype GR_{LBD}(Vel) (human $GR\alpha_{529-777}$ [WT] with velsecorat) was cloned into the pET24a vector (Novagen) featuring an N-terminal His6-tag and a TEV protease cleavage site. The expression vector was transformed into *E. coli* BL21(DE3) STAR, followed by expression in PASM-5052 autoinduction medium. 50 μM velsecorat was added after the cell culture reached an OD of 0.6 followed by expression over 48 hours at 16 °C. All purification buffers were degassed and contained 2 mM TCEP and 20 μM velsecorat. The harvested cells were resuspended in lysis buffer (50 mM Tris pH 8, 10% glycerol, 1% CHAPS) supplemented by protease inhibitors (Complete, Roche) and DNAse. Cells were lysed by sonication. The cleared lysate was applied to a nickel affinity column equilibrated with wash buffer (50 mM Tris pH 8.0, 10% glycerol, 1% CHAPS, 60 mM NaCl) and eluted by a 300 mM imidazole gradient. The purification tag was removed by TEV protease cleavage while dialyzing against a 50 mM Tris buffer at pH 9.0 overnight followed by a second Nickel affinity step to collect the cleaved target protein in the flowthrough. Remaining impurities were removed by size exclusion using 50 mM Tris buffer at pH 9.0, 2 mM TCEP, 20 μM velsecorat as running buffer. The purified protein in 50 mM Tris buffer pH 9.0, 2 mM TCEP, 10 μM velsecorat was flash frozen in liquid N_2 and stored at -80°C.

GRα complex formation with DNA and peptide

Peptides of human peroxisome proliferator–activated receptor γ coactivator 1-α ($PGC1\alpha_{134-154}$: PPQEAEEPSLLKKLLLAPANT) dissolved in water and dsDNA (see below) from the GR DNA response element from the serum and glucocorticoid-regulated kinase-1 (*SGK-1*) were used for complex formation with GRα. The purified ligand bound GRα proteins were mixed with dsDNA (1 : 0.6 ratio of LBD monomer to ds DNA) and peptide (1 : 1.3 ratio of

LBD monomer to peptide) and dialyzed overnight into 20 mM MOPS pH 7.0, 150 mM NaCl, 3mM $MgCl_2$, 0.75 % glycerol, 1 mM TCEP, 10 µM ligand for crystallization or SEC-MALS.

DNA oligonucleotides (Sigma Aldrich) used for *SGK* dsDNA formation:

***SGK* dsDNA**	**Oligo 1**	**Oligo 2**
*SGK*23overhang	*SGK*23oF: 5'-TACAGAACATTTTGTCCGTCGAC-3'	*SGK*23oR: 5'- TCGACGGACAAAATGTTCTGTAC-3'
*SGK*23blunt	*SGK*23bF: 5'-GTACAGAACATTTTGTCCGTCGA-3'	*SGK*23bR: 5'-TCGACGGACAAAATGTTCTGTAC-3'
*SGK*24blunt	*SGK*24F: 5'-GTACAGAACATTTTGTCCGTCGAC-3'	*SGK*24R: 5'-GTCGACGGACAAAATGTTCTGTAC-3'
FAM-*SGK*24	6-FAM-*SGK*24F: 5'-(6-FAM)-GTACAGAACATTTTGTCCGTCGAC-3'	*SGK*24R: 5'-GTCGACGGACAAAATGTTCTGTAC-3

Crystallization and crystal structure determination

The complex $GR_{\Delta N}$(FF)-*SGK*-PGC1α (human $GR\alpha_{385-777}$ [S404A, N517D, V571M, F602S, C638D] with the agonist fluticasone furoate, the dsDNA *SGK*23overhang and the peptide $PGC1\alpha_{134-154}$) was concentrated to approx. 10 mg/mL and crystallization optimized in hanging drops using multiple rounds of seeding. Drops were set up with a 1 : 1 ration of protein complex solution to well solution (8 % PEG3350, 0.1 M Bis-Tris-Propane pH 6.5, 8 % 2,2,2-Trifluoroethanol, 0.1 M Guanidine HCl, 0.3 M Hexanediol). The complex $GR_{\Delta N}$(Vel)-*SGK*-PGC1α with the agonist velsecorat, *SGK*23blunt and the peptide PGC1α was concentrated to approx. 10 mg/mL and crystallization optimized in hanging drops using multiple rounds of seeding. Drops were set up with a 1 : 1 ratio of protein complex to well solution (8.6 % PEG3350, 0.1 M Bis-Tris-Propane pH 6.5, 2 % 2,2,2-Trifluoroethanol, 0.1 M Guanidine HCl,

683 0.3M 1,6-Hexanediol). 30 % ethylene glycol or 30 % glycerol in well solution was used as
684 cryoprotectant and crystals were flash frozen in liquid nitrogen for data collection. Data was
685 collected with a Pilatus3 x 2M detector at the automated beamline ID30A-1/MASSIF-1 at the
686 European Synchrotron Radiation Facility (ESRF).
687 A twofold molar excess of PGC1$\alpha_{134\text{-}154}$ was added to GR_{LBD}(Vel) (human GR$\alpha_{529\text{-}777}$ [WT],
688 co-expressed with velsecorat) and the protein concentrated to 10 mg/mL. Crystals were grown
689 at 20 °C in sitting drops using a 1 : 1 (100 nL + 100 nL) ratio of protein and well solution (18
690 % PEG8000, 2 % 2-Propanol, 0.1 M Sodium acetate, 0.1 M HEPES pH7.5). Crystals were
691 cryo-protected in well solution supplemented with 20 % glycerol and flash frozen in liquid
692 nitrogen. Data was collected with a Pilatus 6M detector at the beamline ID23-1 at the ESRF.
693 All datasets were integrated and scaled with autoPROC (Global Phasing)[5] and initial models
694 obtained performing molecular replacement with the known structures 4P6W and 3G9O using
695 PHASER[6]. The models were improved by iterative rounds of refinement using BUSTER
696 (Global Phasing) [7] and manual model building in COOT[8]. The PyMOL Molecular Graphics
697 System, Version 2.1.0, Schrödinger, LLC, was used to generate figures.
698 Detailed statistics of data collection and refinement can be found in Supplementary Table 1.
699 All coordinates and structure factors have been deposited in the Protein Data Bank (PDB)
700 under the accession codes 7PRV, 7PRW and 7PRX.
701 PDBePISA[9] has been used for interface analysis and Cα root mean square deviation (r.m.s.d.)
702 values calculated with lsqkab[10].
703
704 **Analysis of the sequence conservation of GR**
705 A set of GR-like vertebrate sequences were gathered through iterative Blast searches [11],
706 starting with human GR (NP_000167.1). Sequences with an identity above 50% to the query
707 were aligned with Geneious Prime v. 2021.1.1 using MUSCLE [12]. All entries with an identity

>90% to any other entry in the set were purged, while the least similar sequence to the query was used for subsequent searches. This resulted in a diverse alignment of the GR family with a pairwise sequence identity of 37-84% between all sequences (Extended Data Fig. 3). A set of ER-like vertebrate sequences were gathered by a similar approach, starting with human ER (NP_000116.2) (Extended Data Fig. 4) and purged to match the diversity of the GR set. The mean pairwise column identity of each residue was calculated by Geneious, plotted by Spotfire Analyst 11.4 (Extended Data Figure 3 and 4) and subsequently color mapped onto the GR and ER LBD structures (Fig. 2d, e and Extended Data Fig. 5)

Binding assay to dsDNA in competition mode

The affinity of GR (human WT GR$\alpha_{1\text{-}777}$) in the presence of different ligands to fluorescein (6-FAM) labelled dsDNA FAM-*SGK*24 was analyzed using fluorescence polarization in competition mode.

150 nM GR complexed with the ligands dexamethasone [GR(Dex)], velsecorat [GR(Vel)] or fluticasone furoate [GR(FF)] was mixed with 10 nM FAM-*SGK*24 in HBSP buffer (10 mM HEPES pH 7.4, 150 mM NaCl, 0.005 % Tween-20®). This preformed complex was mixed with a dilution series (1.5 µ, 750 nM, 375 nM, 187.5 nM, 93.75 nM, 46.88 nM, 23.44 nM, 11.7 nM, 5.9 nM and 0 nM) of competing unlabeled dsDNA *SGK*24blunt. Fluorescence polarization was measured using a PHERAStar microplate reader (BMG LABTECH) with the FP Module 485-520/520. IC50 value was determined by simultaneous fitting all curve data (three curve replicates from one experiment) using a four parameter non-linear curve fit in GraphPad Prism 9.

Hydrogen/deuterium exchange mass spectrometry (HDX-MS)

The HDX experiments were carried out using a HDX Manager (Waters) equipped with a CTC PAL sample handling robot (LEAP Technologies). GR (human GR$\alpha_{1\text{-}777}$ [WT]) in the presence of the ligand dexamethasone [GR(Dex)], velsecorat [GR(Vel)] or fluticasone furoate [GR(FF)] and also the complexes GR(Dex)-*SGK*-PGC1α, GR(FF)-*SGK*-PGC1α and GR(Vel)-*SGK*-PGC1α (GR with the dsDNA *SGK*24blunt and PGC1$\alpha_{134\text{-}154}$) were dialyzed into the HDX compatible buffer 20 mM HEPES pH 7.0, 200 mM NaCl, 2.5 % glycerol, 1 mM TCEP, 20 µM ligand and the exchange reactions performed with a CTC PAL sample handling robot (LEAP Technologies). The samples were labelled for 0 s, 30 s, 60 s, 180 s, 600 s and 1800 s by incubating 3 µl protein (GR at 1 mg/mL or GR complexes at 0.6 mg/mL) with 57 µl of D_2O buffer (20 mM HEPES pD 7.4, 200 mM NaCl, 2.5 % glycerol, 1 mM TCEP) at 22 °C. To stop the exchange reaction Quench (3M Urea, 0.1 % TFA, pH2.5) was added 1 : 1 at 4 °C and the mixture was injected onto an online pepsin digestion system with a Waters Enzymate™ BEH Pepsin Column (2.1 x 30 mm, 5 µm) in 0.1 % formic acid in water at 150 uL/min for 3 min at 0.1 °C. The peptides were trapped/desalted for 3 min on a Waters ACQUITY UPLC BEH C18 VanGuard Pre-Column (2.1 × 5 mm, 1.7 µm) and separated on a using a C18 reverse phase column (ACQUITY UPLC BEH C18 Column, 1.7 µm, 2.1 × 100 mm, Waters) by running a linear gradient from 5 - 40 % solvent B (solvent A: 0.1 % formic acid in water; solvent B: 0.1 % formic acid in acetonitrile) over 9 min. The peptides were analyzed on a Waters Synapt G2-Si mass spectrometer, identified using MSE fragmentation. Mass spectrometry experiments acquired over a mass range from 50 to 2000 m/z using an electrospray ionization source operated at a temperature of 200 °C and a spray voltage of 4.5 kV. All reactions were carried out in triplicates and no correction was made for back exchange, therefore all results are reported as relative deuterium exchange levels.

Peptides were identified using the ProteinLynx Global Server 3.0.2 (PLGS, Waters) and deuterium incorporation was analyzed in DynamX 3.0 (Waters). Tables including all peptides with sequences, monoisotopic mass, retention time and mean deuterium uptake is supplied as Extended Data Tables 2 and 3 following guidelines by[13]. Relative deuterium levels were calculated for each peptide by subtracting the average mass of the deuterium-labeled GR with ligand 1 from that of the deuterium-labeled GR with ligand 2. Statistical significance was determined in t tests as p values < 0.05 and listed in Extended Data Tables 4, 5, 6 and 7. Visualization was done using GraphPad Prism 9.

Size exclusion chromatography multi angle light scattering (SEC-MALS)

A Cytiva Superdex® 200 Increase 10/300 GL column on an OMNISEC RESOLVE/REVEAL System (Malvern Panalytical) was used to analyze the absolute molecular weight (MW) of $GR_{\Delta N}$(FF) and $GR_{\Delta N}$(Vel) (human $GR\alpha_{385\text{-}777}$ [S404A, N517D, V571M, F602S, C638D] with the agonist fluticasone furoate or velsecorat) in the buffer 20 mM HEPES pH 7.0, 250 mM NaCl, 2.5 % glycerol, 1 mM TCEP, 10 µM ligand at a flow rate of 0.4 mL/min.

A Cytiva Superose® 6 Increase 10/300 GL column on an OMNISEC RESOLVE/REVEAL System (Malvern Panalytical) was used to analyze the absolute molecular weight (MW) of the complexes $GR_{\Delta N}$(FF)-*SGK*-PGC1α and $GR_{\Delta N}$(Vel)-*SGK*-PGC1α (human $GR\alpha_{385\text{-}777}$ [S404A, N517D, V571M, F602S, C638D] with the agonist fluticasone furoate or velsecorat, the dsDNA *SGK*23overhang or *SGK*23blunt respectively and $PGC1\alpha_{134\text{-}154}$) in the buffer 20 mM MOPS pH 7.0, 150 mM NaCl, 3 mM $MgCl_2$, 0.75 % glycerol, 1 mM TCEP, 10 µM ligand at a flow rate of 0.4 mL/min.

The software OmniSEC5.12 was used to analyze the data with the 3 detector method and to determine the molecular weights of the proteins and protein-DNA-peptide complexes.

Analyzed proteins and protein complexes were also separated on a native PAGE (NuPAGE™ 3 to 8%, Tris-Acetate, Invitrogen).

Inhibition of cytokine (TNF-α) release in whole blood

Whole blood from human with sodium heparin as anticoagulant was used as an anti-inflammatory model to test for steroid like activity (TNF-α inhibition) of GR agonists. A dilution series (1 µM, 0.33 µM, 0.11 µM, 0.037 µM, 0.012 µM, 0.0041 µM, 0.0013 µM, 0.00045 µM) of velsecorat, fluticasone furoate or dexamethasone in DMSO was analyzed. 1 µl of GR agonist was mixed with 190 µL of whole blood and incubated for 45 min at 37°C in 96-well plates. 10 µl LPS, Lipopolysaccharide from E.coli serotype O127:B8 2mg/ml in PBS (SigmaAldrich), was added per well and the plates were incubated overnight at 37°C. The cells were spun down at 1800 rpm for 10 min at 4°C and the culture supernatants stored at -80°C until analysis. The culture supernatants were diluted and added to ELISA plates (R&D Systems) and TNF-α was measured according to the manufacturer's instructions. The raw data in pg/ml was normalized to % inhibition. The IC50 value was determined by simultaneous fitting all curve data (six curve replicates from three donors) using a four parameter non-linear curve fit in GraphPad Prism 9.

Transactivation assay

A reporter vector for GR activity was constructed by cloning the glucocorticoid receptor responsive MMTV promoter upstream of a codon optimized (GeneArt, ThermoFisher Scientific) NanoLuc® Luciferase reporter to replace the CMV promoter in a pcDNA3.1 backbone. A plasmid containing a Firefly luciferase driven by the PGK promoter (#E5011, Promega) was co-transfected and used for normalization.

GR_{WT} (human $GR\alpha_{1-777}$ [WT]) and 6 different GR mutants (GR_{cryst}(S404A, N517D, V571M, F602S, C638D), GR(A458T), GR(R614A), GR(K720D), GR(D641K) and GR(Y640S) were synthesized, codon optimized (GeneArt, ThermoFisher Scientific) and cloned under the control of a CMV promoter into pcDNA3.1.

For transactivation assays COS-7 cells (ECACC 87021302, [14]) were transfected using Lipofectamine 3000 (Invitrogen) according to the manufacturer's instructions and seeded into 384-well OptiPlates (PerkinElmer) at 5000 cells / well and seeded into 6 well plates (620,000 cells /well) for subsequent immunoblotting. Following 24 hours of incubation the 384-well plates were treated with dexamethasone at the indicated concentrations. Reporter gene activation of NanoLuc® and Firefly Luciferase was read out 24 hours later using Nano-Glo® Dual-Luciferase® Reporter Assay System (Promega) according to the manufacturer's instructions. GraphPad Prism 9 was used for data analysis and graph generation. The EC50 value was determined by simultaneous fitting all curve data (eight curve replicates from four experiments) using a four parameter non-linear curve fit in GraphPad Prism 9.

To verify the expression of the different GR mutants in COS-7 cells, immunoblots of the transfected cells were carried out using a rabbit anti-GR-antibody (Cell Signaling, #3660) and a mouse anti-actin antibody (Invitrogen, # MA5-11869). Detection was performed using corresponding secondary antibodies (LI-COR #926-68071; #926-32210). Densitometry quantification was performed using Image Studio Software (LI-COR)(LICOR).

References

1 Galliher-Beckley, A. J., Williams, J. G., Collins, J. B. & Cidlowski, J. A. Glycogen synthase kinase 3beta-mediated serine phosphorylation of the human glucocorticoid

receptor redirects gene expression profiles. *Molecular and cellular biology* **28**, 7309-7322, doi:10.1128/MCB.00808-08 (2008).

2 Bledsoe, R. K. *et al.* Crystal Structure of the Glucocorticoid Receptor Ligand Binding Domain Reveals a Novel Mode of Receptor Dimerization and Coactivator Recognition. *Cell* **110**, 93-105, doi:10.1016/S0092-8674(02)00817-6 (2002).

3 Carlsson, P., Koehler, K. F. & Nilsson, L. Glucocorticoid Receptor Point Mutation V571M Facilitates Coactivator and Ligand Binding by Structural Rearrangement and Stabilization. *Molecular Endocrinology* **19**, 1960-1977, doi:10.1210/me.2004-0203 (2005).

4 Kauppi, B. *et al.* The Three-dimensional Structures of Antagonistic and Agonistic Forms of the Glucocorticoid Receptor Ligand-binding Domain: RU-486 INDUCES A TRANSCONFORMATION THAT LEADS TO ACTIVE ANTAGONISM. *Journal of Biological Chemistry* **278**, 22748-22754, doi:10.1074/jbc.M212711200 (2003).

5 Vonrhein, C. *et al.* Data processing and analysis with the autoPROC toolbox. *Acta Crystallographica Section D* **67**, 293-302, doi:10.1107/S0907444911007773 (2011).

6 McCoy, A. J. *et al.* Phaser crystallographic software. *Journal of Applied Crystallography* **40**, 658-674, doi:10.1107/S0021889807021206 (2007).

7 Bricogne, G. *et al.* BUSTER version *Cambridge, United Kingdom: Global Phasing Ltd.* (2017).

8 Emsley, P., Lohkamp, B., Scott, W. G. & Cowtan, K. Features and development of Coot. *Acta Crystallographica Section D* **66**, 486-501, doi:10.1107/S0907444910007493 (2010).

9 Krissinel, E. & Henrick, K. Inference of Macromolecular Assemblies from Crystalline State. *Journal of Molecular Biology* **372**, 774-797, doi:10.1016/j.jmb.2007.05.022 (2007).

10 Kabsch, W. A solution for the best rotation to relate two sets of vectors. *Acta Crystallographica Section A* **32**, 922-923, doi:10.1107/S0567739476001873 (1976).

11 Altschul, S. F. *et al.* Gapped BLAST and PSI-BLAST: a new generation of protein database search programs. *Nucleic acids research* **25**, 3389-3402, doi:10.1093/nar/25.17.3389 (1997).

12 Edgar, R. C. MUSCLE: multiple sequence alignment with high accuracy and high throughput. *Nucleic Acids Research* **32**, 1792-1797, doi:10.1093/nar/gkh340 (2004).

13 Masson, G. R. *et al.* Recommendations for performing, interpreting and reporting hydrogen deuterium exchange mass spectrometry (HDX-MS) experiments. *Nature Methods* **16**, 595-602, doi:10.1038/s41592-019-0459-y (2019).

14 Gluzman, Y. SV40-transformed simian cells support the replication of early SV40 mutants. *Cell* **23**, 175-182, doi:10.1016/0092-8674(81)90282-8 (1981).

Acknowledgments

We acknowledge the European Synchrotron Radiation Facility for provision of synchrotron radiation facilities and we would like to thank the beamline staff for assistance in using beamline ID30A-1/MASSIF-1 and ID23-1. S.P. and C.K. were supported by the AstraZeneca postdoctoral program. We thank John Steele, Rose Maciewicz, Nils-Olov Hermansson, Matti Lepistö and Richard Neutze for scientific discussions. This work was supported by CNRS, Inserm, Institut National du Cancer (INCa_16099), Fondation pour la Recherche Médicale (FRM), Agence Nationale pour la Recherche (ANR) and the French Infrastructure for Integrated Structural Biology FRISBI ANR-10-INSB-05-01, Instruct-ERIC, and the French Proteomic Infrastructure ProFI ANR-10-INBS-08-03.

Author contributions

S.P. purified the proteins and crystallized the $GR_{\Delta N}$ complexes. C.K. purified the wildtype GR_{LBD} protein. L.W. crystallized the GR_{LBD}. S.P. and K.E. solved the structures and wrote the manuscript with input from all authors. S.P. and C.J. performed HDX experiments and analyzed the data. S.P. and A.G. performed fluorescence polarization assays. S.P., M.C. and E.G. performed SEC-MALS and analyzed the data. P.J. analyzed the sequence conservation of GR and ER. B.C., D.Ö., L.F.R., S.P., K.E., I.D., S.D designed and cloned constructs and performed cell assays. B.B., B.P.K. and I.B.M. helped to conceive and conceptualize the study and interpret structural data.

Competing interests

Sandra Postel, Lisa Wissler, Carina A. Johansson, Anders Gunnarsson, Euan Gordon, Barry Collins, Christian Köhler, Marie Castaldo, David Öling, Patrik Johansson, Linda Fröderberg Roth, Ian Dainty, Stephen Delaney and Karl Edman were employed by AstraZeneca at the time of the study. The authors declare no competing financial interest.

Data availability

The X-ray data and coordinates for the $GR_{\Delta N}$(Vel)-*SGK*-PGC1α, GR_{LBD}(Vel)-PGC1α and $GR_{\Delta N}$(FF)-*SGK*-PGC1α structures are deposited in the PDB (7PRW, 7PRX and 7PRV, respectively). The data will be released upon publication.

Corresponding Author

Karl.Edman@astrazeneca.com